National Aeronautics and
Space Administration

Artemis Campaign Development
ACD-50044
REVISION A

EFFECTIVE DATE: MAY 25, 2023

LUNAR SURFACE DATA BOOK

REVISION AND HISTORY PAGE

Revision No.	Change No.	Description	Effective Date
-	ACD-C0032	Initial Baseline Release (Reference Artemis Campaign Development (ACD) Control Board (ACB), dated 10/06/22)	10/06/22
A	ACD-C0065	Editorial changes throughout; moved section 6.0 to new section 6.1; added content to sections 5.0 and 7.0; added new sections 3.1.1, 3.1.2, 3.2.2 through 3.2.8, 4.4 through 4.12, 5.3, 6.1, 6.2, 6.3, 6.4, 7.3.4, and 7.3.5; expanded section 3.2 beyond LRO; expanded section 4.3; broadened the scope of the traverse sections in 7.3; added content to Appendices A and B; added Appendices D and E; added links to all references; revised and expanded the reference documents list; assigned tracking numbers to baselined TBXs and added several more; reorganized Appendix C.	05/22/23

TABLE OF CONTENTS

SECTION **PAGE**

1.0 INTRODUCTION

1.1 PURPOSE

Artemis missions will need to reference and work with a common set of lunar surface data, products, and analytical assumptions to accomplish Artemis mission science, exploration, and operational objectives. This Lunar Surface Data Book is intended to be used as a reference for candidate vendors and agency personnel who are addressing Artemis lunar surface challenges to ensure a common set of data sources and assumptions when interpreting remote sensing data specific to the needs of surface mission planning.

1.2 SCOPE

This document provides a common reference set of existing lunar surface data, products, analytical assumptions, and representative use cases to be incorporated into Artemis surface mission planning efforts. This document pertains solely to the surface of the Moon and the ecosystem of data and products to be used to describe the lunar surface. The focus of this document is the lunar south pole region, defined in the 2020 NASA Lunar Exploration Plan (more formally, NASA's Lunar Exploration Program Overview) as the region within six degrees latitude of the geographic lunar south pole. It is the region selected for long-term stays.

1.3 CHANGE AUTHORITY/RESPONSIBILITY

NASA Office of Primary Responsibility (OPR) identified for this document is ACD Systems Engineering & Integration (SE&I). Proposed changes to this document shall be submitted via a Change Request (CR) to the appropriate ACD Control Board for consideration and disposition. All such requests shall adhere to the ACD Configuration Management Process documented in ACD-50005, ACD Configuration and Data Management Plan.

2.0 DOCUMENTS

2.1 APPLICABLE DOCUMENTS

The following documents include specifications, models, standards, guidelines, handbooks, and other special publications. The documents listed in this paragraph are applicable to the extent specified herein.

Document Number	Document Title
SLS-SPEC-159	Cross Program Design Specification for Natural Environments (DSNE)

2.2 REFERENCE DOCUMENTS

The following documents contain supplemental information to guide the user in the application of this document. Additional references to data sources in this document can be found in Appendix B.

Document Number	Document Title
EHP-10033	EHP Integrated Concept of Operations
ESDMD-001	Moon-to-Mars Architecture Definition Document
ESDMD-410	Lunar Surface Exploration Planning: Terrain Characteristics
EVA-EXP-0042	Extravehicular Activity (EVA) Office Exploration EVA Systems Concept of Operations
HLS-CONOP-001	HLS Concept of Operations - Initial Phase Mission
HLS-CONOP-006	Sustained Phase HLS Concept of Operations
HLS-CONOP-007	Human-Class Delivery Lander Concept of Operations
LTV-CONOPS-001	Lunar Terrain Vehicle (LTV) Project Concept of Operations
NP-2020-05-2853-HQ	NASA's Lunar Exploration Program Overview

3.0 LUNAR SURFACE DATA SOURCES

SLS-SPEC-159 Cross-Program Design Specifications for Natural Environments (DSNE) is the baseline source for all natural lunar environments. The DSNE is a mandatory engineering technical authority document and is fully applicable to the Artemis Campaign. The DSNE contains lunar surface environment characteristics for surface hardware design and verification. The Lunar Surface Data Book complements the DSNE with additional site-specific characteristic data, products, analytical assumptions, and representative use cases.

Between 1963 and 1972, the Moon was a focus of an intense, integrated program of American exploration including robotic orbiters (Lunar Orbiter) and impactors (Ranger), soft landers (Surveyor) and crewed missions (Apollo). In the 21st century, an ambitious flotilla of international missions has developed a modern view of the Moon and its surface. These modern missions (e.g., the Japan Aerospace eXploration Agency (JAXA) Kaguya, European Space Agency (ESA) Smart 1, NASA/Department of Defense (DOD) Clementine, NASA Lunar Prospector, Indian Space Research Organisation (ISRO) Chandrayaan-1, NASA GRAIL (Gravity Recovery and Interior Laboratory), NASA LADEE (Lunar Atmosphere and Dust Environment Explorer), NASA LCROSS (Lunar Crater Observation and Sensing Satellite), and NASA Lunar Reconnaissance Orbiter (LRO) have all dramatically increased our understanding of the Moon's environment. Therefore, the Moon is the one planetary object besides Earth that has been systematically studied for over five decades from a variety of perspectives including remote observations, in situ measurements, human field work, and returned samples with appropriate geological context. With that full suite of data sources, lunar scientists and mission planners today have access to several data sources and products that characterize the lunar surface, making the Moon the most well-understood and well-characterized body in our solar system besides Earth. That relative wealth of knowledge compared to other solar system objects, especially when compared to the spartan state of our knowledge prior to the Apollo missions, enables 21st century lunar mission planners to optimize systems, do detailed mission planning, and enable transformative lunar science and exploration outcomes with future missions. This section describes the sources of data before reviewing the data themselves and only the most recent and relevant data is included.

This document presents a compilation of data readily available in NASA's Planetary Data System and other data repositories with source data and detailed explanations as well as data interpretation available in peer-reviewed literature. Future Science Mission Directorate (SMD) Lunar Discovery and Exploration Program missions to the lunar poles will improve our understanding of lunar surface characteristics, but those missions have not yet occurred and presently play no role in mission planning. The emphasis in this document is placed on the data from US missions, particularly that from the Lunar Reconnaissance Orbiter, because the provenance of those data is well-understand and fully characterized, and all Lunar Reconnaissance Orbiter source data is fully and publicly available per long-standing NASA Policy.

3.1 IN SITU LUNAR SURFACE DATA

A robust set of surface data exists for the multiple landing sites visited by NASA missions (Surveyor and Apollo). Data for surface (regolith) geotechnical and rock abundance properties is derived from both images/observations and physical measurements of the surface. The Lunar Sourcebook (Heiken et al., 1991) includes geotechnical data from the Soviet Lunokhod 1 and 2 uncrewed rovers that traversed 47 km of the lunar surface and collected on the order of 1000 cone vane penetrometer measurements of the upper 10 centimeters of the regolith. Much of the data from the 1960 and 1970s is not in modern formatting, only preserved as film negatives or tabular data formats. That said, the in-situ data presents our best understanding of the specific properties of the lunar surface which are directly applicable to Artemis mission planning. Given that, care must be used to not over-interpret landing site data that is NOT relevant to the lunar south pole. For example, much consternation could arise from assuming any site is similar to the rocky surface encountered by the Surveyor VII mission, which landed (autonomously) and without any active hazard avoidance in the rockiest region yet explored on the Moon. We have no reason to believe the south pole region will be in any way similar to that particular landing site. Instead, Artemis landing sites will be in the lunar highlands of the south pole region, resulting in operations much more comparable to the Apollo 14 and 16 landing sites. Data from these missions are available through NASA's Planetary Data System (PDS) (https://pds.nasa.gov/), NASA's Space Science Data Coordinated Archive (NSSDC) (https://nssdc.gsfc.nasa.gov/), and the Analyst's Notebook (https://an.rsl.wustl.edu/). Links to data sets are provided in each individual subsection that follows.

3.1.1 Apollo Data

Reserved. **<TBD-ACD-50044-008>**

3.1.2 Lunokhod and Other Robotic Missions

Reserved. **<TBD-ACD-50044-009>**

3.2 ORBITAL DATA RELEVANT TO THE SURFACE

3.2.1 Lunar Reconnaissance Orbiter (LRO)

NASA has sent numerous missions to lunar orbit to understand the lunar surface and its environment, leading to the largest volume of data for any planetary body outside of the Earth. This document focuses on the data that is directly related to the lunar surface and the properties that are derived from them. The most recent and directly relevant source of data on the lunar surface is from the Lunar Reconnaissance Orbiter, sent to the Moon with the explicit goal of developing the data needed to support landing site selection and validation. Since 2010, LRO has been in a stable frozen orbit with periapsis centered on the South Pole, enabling a significantly longer mission duration. A substantial amount of data is now available for the south polar region, giving us the best possible dataset to identify the scientifically interesting and relatively safe sites to explore.

The Lunar Reconnaissance Orbiter was launched on 18 June 2009 from what is now Cape Canaveral Space Force Station and remains in lunar orbit and operational as of January 2023 with funded operations until at least October 2025, spacecraft health non-withstanding. LRO was designed to meet the requirements of the former Exploration Systems Mission Directorate (ESMD) to identify safe landing sites for human and robotic missions to the Moon, understand the lunar radiation environment, and characterize potential lunar resources. After arriving at the Moon in 2009, LRO spent several months in an elliptical, stable frozen 30 x 216 km orbit with apoapsis over the lunar south pole, then transitioned for the next two years into a 50 x 50 km circular polar mapping orbit. Following the completion of its baseline mapping mission in 2010, LRO transitioned into a quasi-stable 30 x 216 km polar orbit which has slowly evolved to a nearly circular 100 km orbit, where it remains today (2023). Despite the natural procession of the orbit away from direct south polar overflights, it is still possible that additional Lunar Reconnaissance Orbiter Camera images can be targeted for select areas in the polar regions; please contact the LRO Project Scientist for additional information using the formal data request process in Appendix D. The LRO mission instrument suite and scientific outcomes have been well-described in multiple publications, including Vondrak et al. 2010 and Keller et al. 2016. LRO carries seven instruments, each designed to investigate a specific aspect of the lunar environment relevant to future exploration. We briefly summarize the LRO instrument suite in this section.

3.2.1.1 The Cosmic Ray Telescope for the Effects of Radiation (CRaTER)

The primary goal of CRaTER is to characterize the lunar radiation environment in terms of the different types of charged particles and their energies, particularly above 10 MeV, to better understand what hazards future human explorers will be subjected to. Radiation comes from the Sun and beyond the Solar System (galactic cosmic rays). These data have allowed scientists to determine the potential biological impacts of the radiation. CRaTER also tests models of radiation effects and shielding and measures radiation absorption by human tissue-like plastic, aiding in the development of protective technologies to help keep crews safe. CRaTER data is available through the NSSDC Master Catalog (https://nssdc.gsfc.nasa.gov/nmc/).

3.2.1.2 Diviner Lunar Radiometer Experiment (DLRE)

The objective of DLRE (more commonly referred to as Diviner) is to measure lunar surface temperatures at scales that provide essential information for future surface operations and exploration. The temperature of the lunar surface and subsurface is a critical environmental parameter for future human and robotic exploration. While the Apollo missions were all targeted to equatorial landing sites and were only conducted during the lunar day, NASA’s new lunar exploration program will involve exploration of much higher latitudes eventually involving astronaut stays of longer than two weeks. A key Diviner objective is to determine the temperatures within Permanently Shadowed Regions (PSRs), to understand the potential of these areas to harbor water ice. Orbital thermal mapping measurements also provide detailed information on surface parameters such as composition, hazards, rough terrain, or rocks. The Diviner instrument can determine surface temperatures to within 5 °C across areas as small as 300 m using 9 different wavelengths between 7 and 200 microns.

Diviner seasonal bolometric temperature data products are commonly used for preliminary evaluation of polar regions of interest. These include the Maximum, Average, Minimum and Amplitude maps at 240 meters per pixel (Williams et al., 2019). The data product descriptions and links to seasonal and hourly temperature products are available from the project team’s website:

Data | diviner (https://www.diviner.ucla.edu/data)

Index of /~jpierre/diviner/level4_polar/additional_maps (https://luna1.diviner.ucla.edu/~jpierre/diviner/level4_polar/additional_maps/)

The seasonal temperature variations are described in detail and mapped by Williams et al (2019), available here: https://doi.org/10.1029/2019JE006028.

The Diviner data is available from the PDS archive at different levels of processing~~.~~:

PDS Geosciences Node Data and Services: LRO Diviner (https://pds-geosciences.wustl.edu/missions/lro/diviner.htm)

3.2.1.3 Lyman Alpha Mapping Project (LAMP)

LAMP is an imaging ultraviolet spectrometer, detecting UV light between 1200 and 1800 Å with an effective surface spatial resolution of up to 200 m per pixel near the poles (Gladstone et al. 2010). The goal of LAMP is to map the entire lunar surface in the far ultraviolet part of the spectrum, including areas in permanent shadow. LAMP searches for surface ice and frost in the polar regions, providing images of permanently shadowed regions illuminated only by starlight and the glow of interplanetary hydrogen emission, known as the Lyman Alpha line. LAMP data is available through the NSSDC Master Catalog (https://nssdc.gsfc.nasa.gov/nmc/).

3.2.1.4 Lunar Exploration Neutron Detector (LEND)

LEND is a neutron spectrometer similar to another instrument, the High Energy Neutron Detector (HEND) on the Mars Odyssey spacecraft. LEND indicates the distribution of surface and subsurface hydrogen through interpretations of detections of the epithermal neutron flux (0.4 eV - 100 eV) at various spatial resolutions depending on orbital altitude. Due to LRO's polar orbit configuration, LEND data is densest, and therefore of highest resolution, in areas around the south pole. The LEND data has been useful for identifying areas of possibly enhanced hydrogen abundance, of interest for future in-situ resource utilization. Refer to LEND papers Mitrofanov et al (2010) and Sanin et al (2017). LEND data is available through the NSSDC Master Catalog (https://nssdc.gsfc.nasa.gov/nmc/).

3.2.1.5 Mini-RF

Mini-RF (Raney et al, 2011) was an advanced synthetic aperture radar, capable of measurements in X-band and S-Band, designed to provide observations of the permanently shadowed areas on the Moon using radar illumination at resolutions of 30 and 150 meters. The intent of the Mini-RF experiment was to determine whether ice was present in significant quantities in the lunar polar regions, as well as to map rock distributions on the lunar surface and subsurface. The instrument no longer has the capability to transmit radar signals, only to receive them. Therefore, it now operates in a receive-only mode measuring bistatic radar signals transmitted from ground-based radio telescopes and reflected off the lunar surface. Mini-RF data is available through the NSSDC Master Catalog (https://nssdc.gsfc.nasa.gov/nmc/).

Data from Mini-RF has been used to study crater geology and mineralogy, as well as material in PSRs of deep polar craters. Refer to Mandt et al, 2016.

3.2.1.6 Lunar Orbital Laser Altimeter (LOLA)

The LOLA instrument (Smith et al. 2010) pulses a single laser at 1064 nm wavelength, splitting the output into five separate beams that illuminate the lunar surface 28 times per second. For each beam, LOLA measures the time of flight (range), pulse spreading (surface roughness), and transmit/return energy (surface reflectance). This allows the topography to be determined, along with an indication of whether the surface is rough or smooth at scales relevant for Exploration planning. LOLA is the "fundamental" dataset for all LRO instruments, providing the foundational global lunar topographic model and geodetic grid that will serve as the framework to enable precise positioning, safe landing, and surface mobility, as well as characterizing the polar illumination environment. LOLA data is available through the NSSDC Master Catalog (https://nssdc.gsfc.nasa.gov/nmc/).

3.2.1.7 Lunar Reconnaissance Orbiter Camera (LROC)

LROC consists of three cameras (Robinson et al., 2010). There are two Narrow Angle Cameras (NACs) that provide panchromatic images over a 5-km swath from the 50km nominal mapping orbit, with resolutions varying from 0.5 to 3 meters per pixel, depending on orbital altitude. There is also a Wide-Angle Camera (WAC), which provides multispectral images with a pixel scale of 100 meters per pixel over seven color bands with a 60 km swath. LROC is designed to address fundamental exploration objectives, including:

- Characterize potential landing sites at the meter scale
- Map regions of permanent shadow or illumination
- Create high-resolution maps of the surface, including polar massifs with near-permanent illumination
- Observe regions from multiple angles to derive high-resolution meter-scale topography
- Map the global distribution of the mineral ilmenite (a key lunar resource)
- Create a global morphology base map
- Characterize lunar regolith
- Establish impact rates for hazard analysis (impactor type requires instrument advancements)

LROC image data is available through the NSSDC Master Catalog (https://nssdc.gsfc.nasa.gov/nmc/).

3.2.2 Clementine

Reserved. **<TBD-ACD-50044-010>**

3.2.3 Lunar Prospector

Reserved. **<TBD-ACD-50044-011>**

3.2.4 Kaguya

Reserved. **<TBD-ACD-50044-012>**

3.2.5 LCROSS

Reserved. **<TBD-ACD-50044-013>**

3.2.6 GRAIL

Reserved. **<TBD-ACD-50044-014>**

3.2.7 Chandrayan 1 and 2

Reserved. **<TBD-ACD-50044-015>**

3.2.8 Danuri (KPLO)

Reserved. **<TBD-ACD-50044-016>**

4.0 LUNAR SURFACE DATA PRODUCTS

4.1 FOUNDATIONAL PRODUCTS

Foundational lunar surface data products are essential descriptive elements built from the raw data collected by instruments described in Section 3. Foundational data products for lunar exploration have recently been described by Laura and Beyer (2021) and the joint Lunar Exploration Analysis Group (LEAG) and Mapping and Planetary Spatial Infrastructure Team (MAPSIT) Lunar Critical Data Products Specific Action Team (LEAG-MAPSIT, 2021). Some definitions of key foundational products are briefly summarized here based upon those sources. The intent of this section is to succinctly describe existing data products that are presently being used for mission planning purposes and provide information on relevant descriptive peer-reviewed publications and expedited ways of accessing relevant source data products.

4.2 VISIBLE IMAGERY & ALTIMETRY

While many subclassifications are possible, in general, visible wavelength imagery of the lunar surface (meaning observations produced by sensors designed to collect data in the visible spectrum wavelengths from 380 to 750 nanometers) can be broken down into three categories. The first two categories, Nadir Imagery (described in section 4.2.1) and Oblique Imagery (described in section 4.2.2), are defined based on the geometry of the camera relative to the surface from orbit. The third category, Image Mosaics (described in section 4.2.3), involves executing geodetic and cartographic processing to combine many smaller images into a larger mosaic useful for precision mapping and analyses. Figure 4.2.1 provides an idealized representation of sensor orientation relative to image geometries.

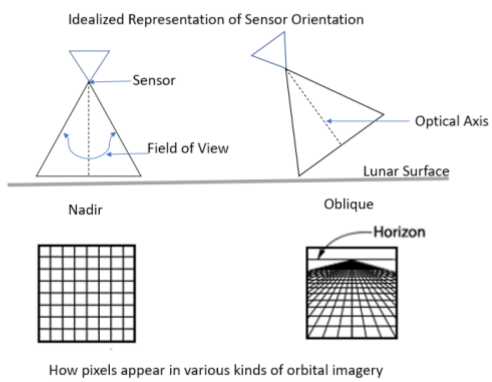

Figure 0.1 Definitions of Sensor Orientation

4.2.1 Nadir Imagery

Nadir imagery is captured from orbit where the camera lens is directly pointing down the nadir direction to the surface. The Narrow Angle Cameras aboard LRO are examples of body-fixed imaging systems whose default mode of operation is a nadir orientation. Figure 4.2.2 is an example of nadir imagery produced by the LROC system.

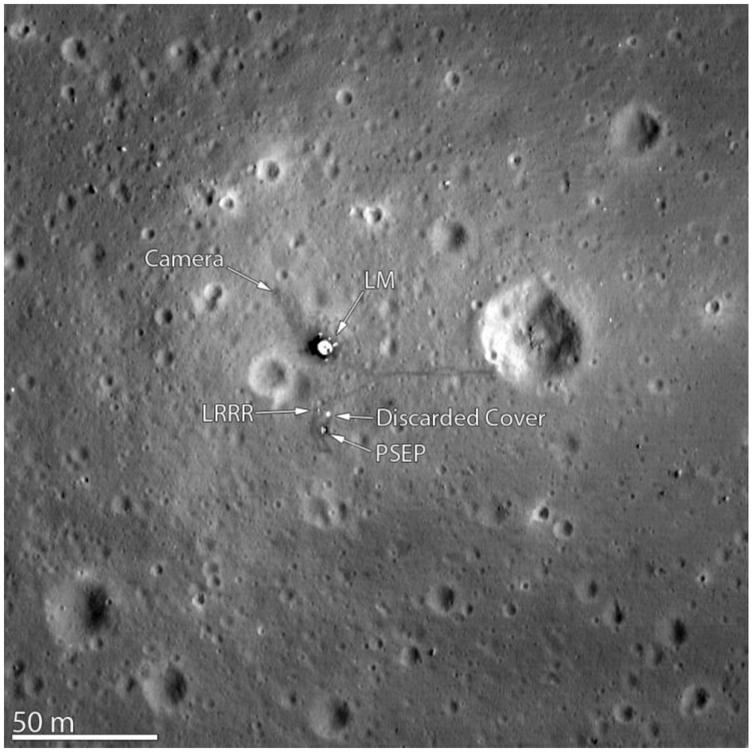

Figure 0.2 Annotated example nadir image of the Apollo 11 landing site and human artifacts at Statio Tranquillitatis (Tranquility Base), imaged by LRO in 2011. The remnants of Armstrong and Aldrin's historic first steps onto the lunar surface are seen as dark paths.

4.2.2 Oblique Imagery

Orbital imagery is captured when the orbiting camera lens is canted off the surface normal, resulting in an oblique angle. Although LROC is a body-fixed, nadir pointing instrument, with sufficient advance planning, LRO has the capability to roll the spacecraft to obtain oblique images with its Narrow Angle Camera system useful for context interpretation and validating lighting models. An example of an oblique image is provided as figure 4.2.3 below.

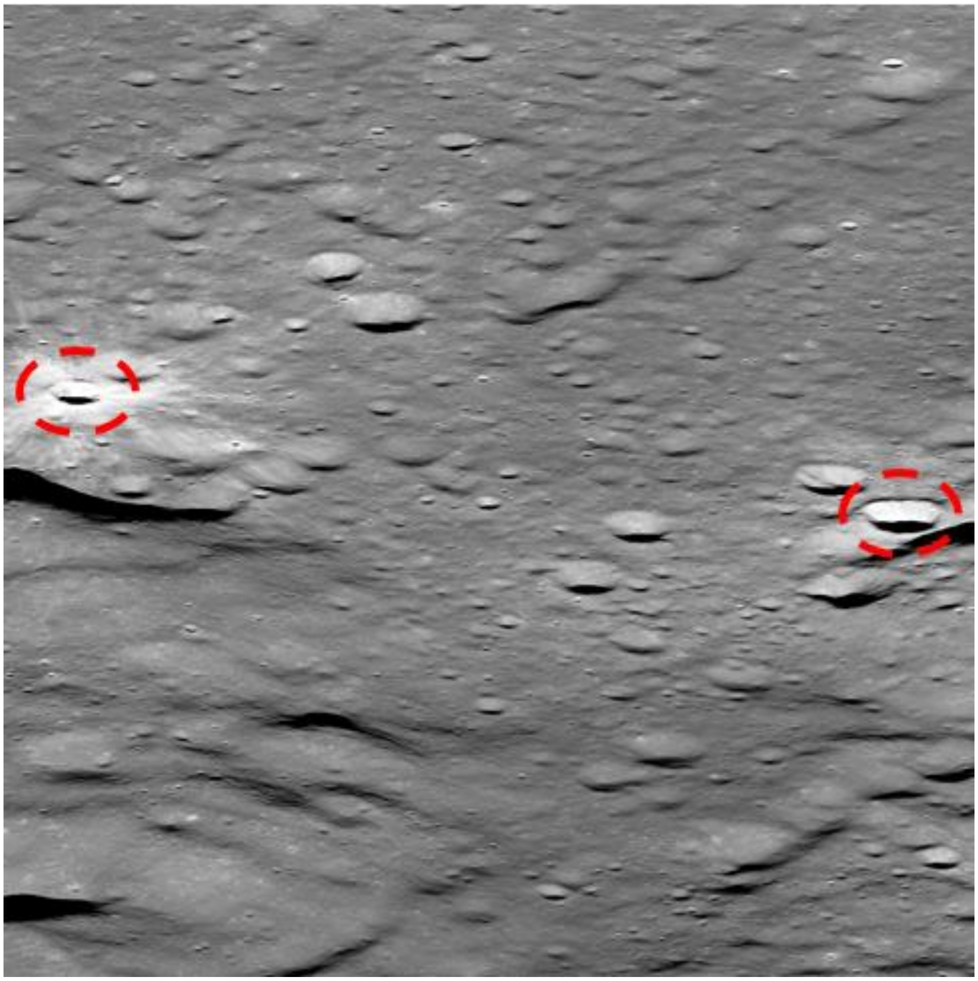

Figure 0.3 Oblique LROC NAC image of the Apollo 16 landing site. Viewpoint is east to west. South Ray crater is center left and North Ray crater is center right. Distance between the two center craters is 10.5 km. Subset of LROC NAC M192817484LR [NASA/GSFC/Arizona] ***(dashed circles in red added to help identify them)***

4.2.3 Mosaics

A visible imagery mosaic is an assemblage of overlapping remotely sensed visible wavelength images whose edges have been matched cartographically to create a continuous photographic representation of a portion of the Moon's surface. There are two broad subcategories of image mosaics, uncontrolled and controlled mosaics.

4.2.3.1 Uncontrolled Mosaics

An uncontrolled mosaic is comprised of images collected under consistent illumination conditions, and whose edges have been matched from image to image without reference to established geodetic control. Seams between distinct images may or may not be visible. An example of an uncontrolled mosaic is provided as Figure 4.2.4 (notice seams are visible in this Figure). An uncontrolled mosaic of the south polar region has been assembled by the LRO

Science Team using LRO NAC images and can be downloaded from the LROC subnode of the PDS Imaging and Cartographic Sciences Node (Viewing South Pole NAC Mosaic (https://wms.lroc.asu.edu/lroc/view_rdr/NAC_POLE_SOUTH))

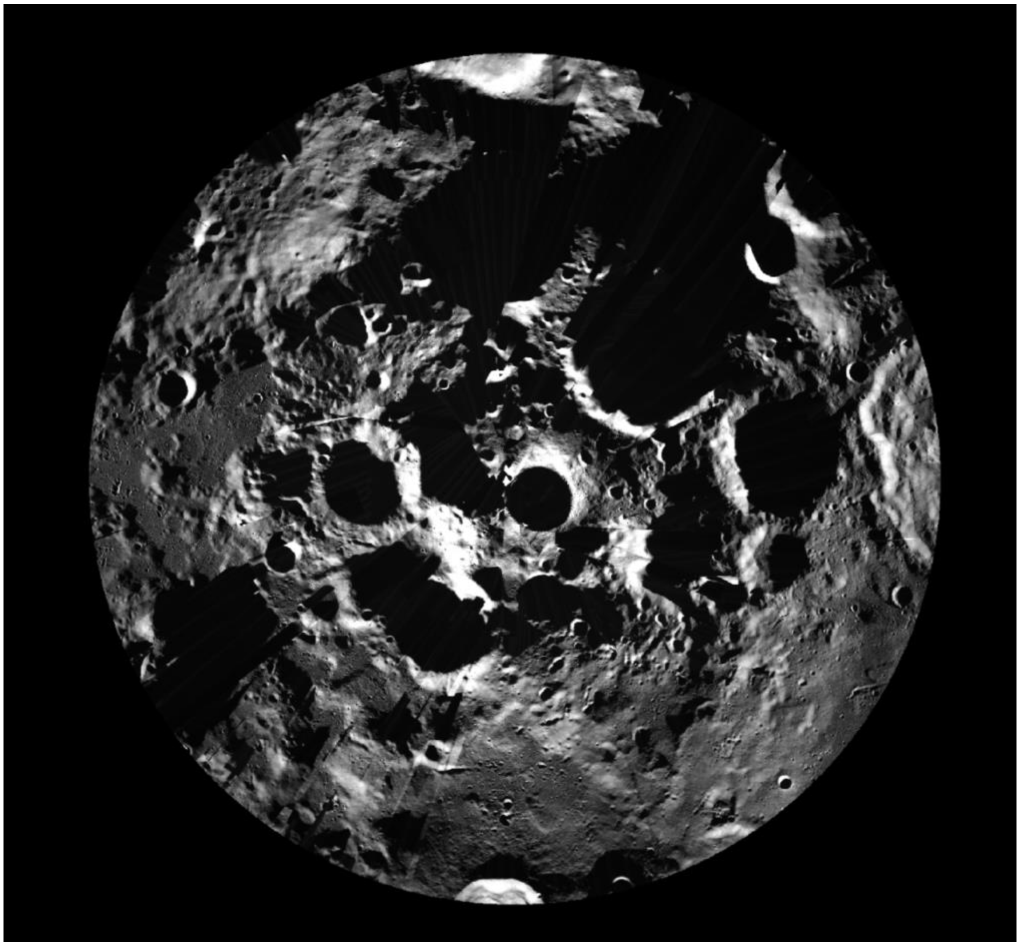

Figure 0.4 Uncontrolled mosaic of 1293 LROC NAC images of the south pole of the Moon, projected in polar stereographic, with a scale of 1 m/pixel from 85.5 - 90 degrees S.

4.2.3.2 Controlled Mosaics

Controlled visible imagery mosaics are mosaics comprised of images that have been radiometrically, geometrically, and photometrically corrected to establish an accurate cartographic framework for regional areas of interest (e.g., Martin et al., 2019). Controlled mosaics produced by the LRO team are referred to as Feature Mosaics and are comprised of NAC images created on sequential orbits. The geodetic control process reduces locational uncertainty and ensures accurate distances can be measured from surface features found within the mosaic. An example of a controlled mosaic from a nonpolar region is provided as Figure 4.2.5. Controlled mosaics of LROC WAC frames for the south polar region have been produced by the LROC team (https://wms.lroc.asu.edu/lroc/view_rdr/WAC_ROI_SOUTH_SUMMER) and the US Geological Survey (available online at https://trek.nasa.gov/moon).

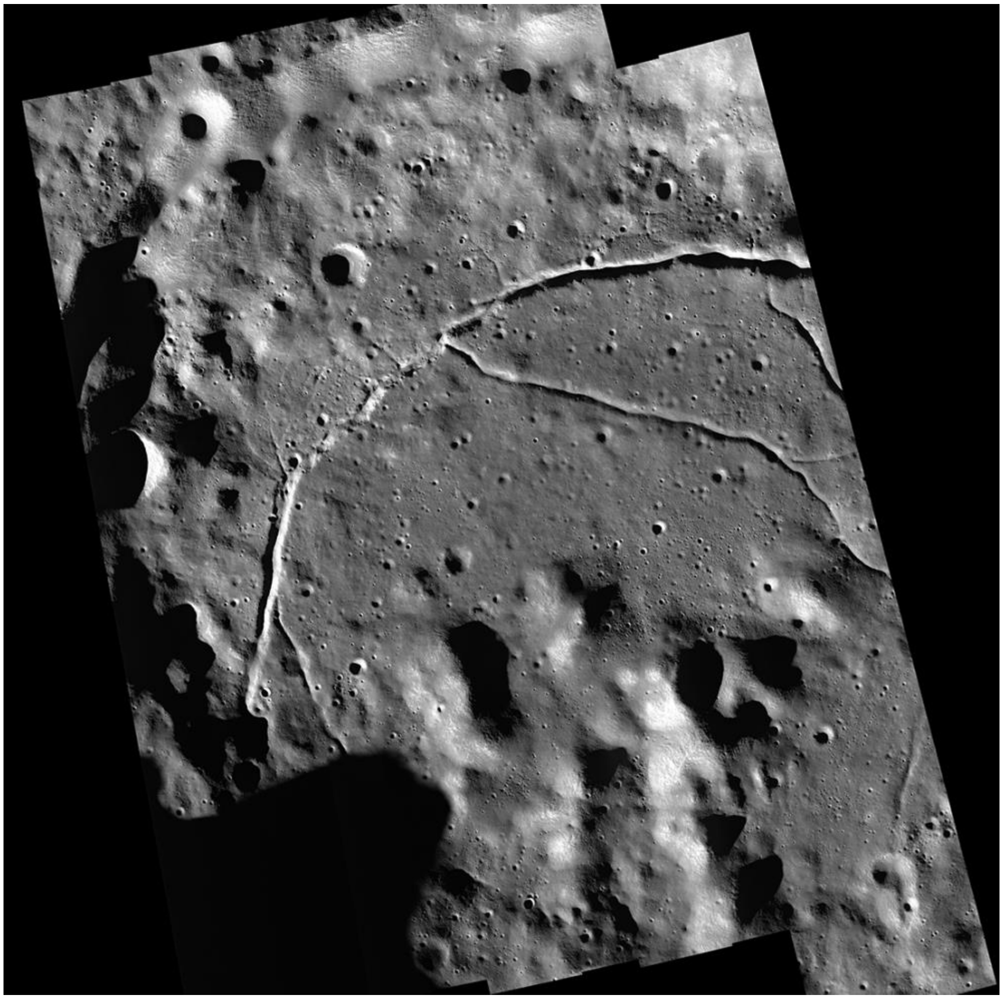

Figure 0.5 A seamless mosaic of a portion of Karpinsky crater (72.61 degrees N, 166.80 degrees East). Scene is 55 km across. NAC images M130949659L/R, M1309503618L/R, M1309510644L/R, M1309517669L/R.

4.2.4 Topographic Data Products

The shape of the lunar surface is described within several complementary topographic data products. Several high-quality topographic products are available for the lunar south pole described below. Topography is one of three primary classes of foundational data products as described in Laura and Beyer (2021).

Generally, there are three categories of terrain models, defined as follows:

- **Digital Elevation Model (DEM):** A digital representation of the topographic surface of a body that excludes natural or built surface objects.

- **Digital Terrain Model (DTM):** A digital representation of the topographic surface of a body that excludes natural or built surface objects but does include natural/built features as vector features.

- **Digital Surface Model (DSM):** A digital representation of the topographic surface of a body, including natural or built surface objects.

Currently, the lunar south pole does not host built surface objects. Preliminary mapping of natural surface objects has begun, but is not yet formalized. For this reason, current topographic products are typically DEMs, although this is expected to change with future surface characterization and activity. Topographic products from several sources are described in the following subsections. Where topographic products are not available or do not provide sufficient resolution, synthetic terrain models may be generated using the statistical descriptions of the lunar surface found in DSNE Section 3.4.1.

4.2.4.1 South Pole LOLA DEM Mosaic

The shape of the lunar surface is directly measured from orbit by the Lunar Orbiter Laser Altimeter. Point measurements are then interpolated into gridded data products. Because of the orbit of LRO, LOLA points are densely clustered at high latitudes, enabling gridded topographic maps at 5 meters per pixel resolution covering much of the South Pole.

This 5 m/pixel product represents a significant improvement over previous LOLA releases. By iteratively co-adjusting the LOLA tracks in a self-consistent fashion, orbital errors were reduced by over a factor of 10 such that the new track geolocation uncertainty is about 10 to 20 cm horizontally and about 2 to 4 cm vertically over each region. The new 5 m/pixel Lunar Digital Elevation Model (LDEM) is substantially more realistic than previous products with fewer artifacts due to orbital errors and fewer spurious noise points. While the fraction of interpolated 5-meter pixels in this polar LDEM is necessarily large (about 90%) due to LOLA's cross-track and inter-spot spacing, this LDEM has the advantages of having accurate geodetic control and being unaffected by shadows, and, thus, will be complementary to higher-resolution topographic models derived solely from imagery.

This product was constructed from 97 individual 20 x 20 km fields with 2 km overlaps. Each field was processed with the same method as described in Barker et al. (2021). The fields were then individually aligned to the original DEM with a rigid 3-D translation and blended with a cosine taper weight in the overlap regions. The LOLA count maps of the individual fields were blended in the same way. Hence, non-integer counts exist in the overlap regions of the final assembled mosaic product.

The LDEM height and slope uncertainties have a stated median RMS-Z error about 0.30 to 0.50 m (see Barker et al (2021) for a full description of source data and error deviation). Interpolation error depends primarily on gap size, or areal density of the LOLA points, with a secondary dependence on terrain slope that becomes more important over highly sloped terrain. Hence, the interpolation error will be larger at greater distances from the pole for the same pixel scale, because of the lower point density and poorer effective resolution.

Metadata products such as count maps and RMS error maps are available. Interpolation errors are quantifiable and manageable.

The LOLA DEM products are the foundation for all LRO data products; all LROC images are controlled to the LOLA dataset.

A mosaic covering all latitudes poleward of 87 degrees S is available in the Planetary Geodesy Data Archive (PGDA), here:

PGDA - South Pole LOLA DEM Mosaic (https://pgda.gsfc.nasa.gov/products/81)

Several additional sites of interest are available here:

PGDA - High-Resolution LOLA Topography for Lunar South Pole Sites (https://pgda.gsfc.nasa.gov/products/78)

A full description of data source calibration/corrections and error deviations is available in Barker et al (2021).

Additional LOLA DEM products covering the wider polar regions are available through the Planetary Data System (https://pds-geosciences.wustl.edu/lro/lro-l-lola-3-rdr-v1/lrolol_1xxx/data/lola_gdr/polar/).

4.2.4.2 LROC NAC DTM: Stereo Observations

The two Narrow Angle Cameras aboard LRO were not designed as a stereo imaging system. However, stereo observations can be acquired over two or more orbits by slewing the spacecraft (Robinson et al., 2010). Globally, a number of these “stereo pairs" have been collected, comprising approximately 3% of the lunar surface. As described in Henriksen et al. (2017), these pairs are then reduced into Digital Terrain Models at the 2 to 4 meters per pixel scale using a consistent set of procedures leveraging the SOftCopy Exploitation Toolkit (SOCET SET) software from BAE systems in combination with the United States Geological Survey (USGS) Integrated Software for Imagers and Spectrometers (ISIS) (Anderson et al., 2004, and Keszthelyi et al., 2013). By enabling quantitative investigations of elevation, slope, volume, and roughness, complex scientific questions and engineering site suitability assessments can both be comprehensively addressed, rendering NAC DTMs invaluable for both engineering and scientific purposes.

These products offer spatial resolution of up to 2 to 4 meters per pixel, with vertical accuracy of less than 1 meter and horizontal accuracy of less than 10 meters.

As of May 2022, three LROC NAC stereo observations have been processed and published in publicly available DTMs and can be downloaded from the LROC subnode of the PDS Imaging and Cartographic Sciences data node:

Terrain Between Nobile and Malapert craters (https://wms.lroc.asu.edu/lroc/view_rdr/NAC_DTM_NOBILE01).

Peak near Spudis crater on the Shackleton-deGerlache connecting ridge (https://wms.lroc.asu.edu/lroc/view_rdr/NAC_DTM_SHACKRDGESM).

Malapert Massif (https://wms.lroc.asu.edu/lroc/view_rdr/NAC_DTM_ESALL_MP1).

In addition, as a deliverable for project Constellation, NAC stereo observations for a large area comprising the rim of Shackleton over to the peak near the rim of Spudis crater have been processed and published as a large high-resolution DTM with 4 meter postings, which can be

downloaded here:
https://astrogeology.usgs.gov/search/map/Moon/LRO/MOON_LRO_NAC_DEM_89S210E_4mp

There is limited potential to collect the additional observations required to enable the creation of additional polar DTMs in other locations near the geographic lunar south pole because of LRO orbital constraints. To request additional LROC imagery of the south polar region, use the data request process in Appendix D.

4.2.4.3 LROC NAC DEM: Photoclinometry

The principle of photoclinometry, also called "Shape from Shading" or SfS, is that nadir images with different lighting conditions (solar incidence and azimuth) can enable mathematical solutions to determine the shape and topography of the illuminated surface. As described by Alexandrov and Beyer (2018), SfS can be used to establish Digital Terrain Models from NAC frames with consistently higher spatial resolution (about 1-2 m/pixel) than that provided by the conventional SOCET SET approaches described in Section 4.2.4.2. These are produced using NAC images and photoclinometry processing, with the LOLA 5 m/pixel product as a basis. This product reverts to LOLA data for unilluminated areas in NAC images.

The quality of this product, which includes an SfS DTM, a maximally lit orthomosaic, and individual orthoimages of each imported NAC image, is limited by the availability of NAC coverage and illumination conditions. A small number of SfS models have been created to support uncrewed NASA missions to the poles, but as of this writing these SfS models are not available for download or use. However, the creation of additional SfS models can be supported if sufficient NAC images with appropriate properties are available for the region of interest; please contact the Artemis Spatial Data Lead, or the SfS model development lead, for additional information, using the data request process in Appendix D.

4.3 DERIVED IMAGERY & ALTIMETRY PRODUCTS

Derived products are created by leveraging foundational products to interrogate or emphasize specific attributes of the surface. Software packages exist, such as Geospatial Data Abstraction Library (GDAL (https://gdal.org/index.html)), that can programmatically generate the products from topographic data. For example, see gdaldem (https://gdal.org/programs/gdaldem.html) for instructions on how to create the products discussed in this section. Products and methods that are already created for the lunar south pole are provided where available.

4.3.1 Slope Map

Slope maps are raster products that capture the angle between the observed surface and a horizontal reference plane. These can be derived from any topographic data product using a variety of algorithms at the desired spatial baseline. Slope maps can be used to identify surface hazards relevant to terrain use as well as to characterize geological attributes.

Slope maps for the lunar south pole (latitudes > 87 deg. S) are currently available at 5 m/pixel, derived from the South Pole LOLA DEM Mosaic (described in Section 4.2.4.1). These maps used Horn’s Method, a standard averaging method to calculate slope from eight neighboring cells/pixels about a center cell/pixel where a third-order finite difference equation is used to produce an estimate of an average slope within that 8-cell neighborhood of a central cell. Full lunar south pole maps are posted here:

PGDA - South Pole LOLA DEM Mosaic (https://pgda.gsfc.nasa.gov/products/81)

Slope maps for individual sites of interest at 5 meters per pixel were derived using a different method. For these maps, slope was calculated as arccos(Nz) where Nz is the z-component of the unit-normal surface vector. The unit-vector is computed with Matlab's surfnorm routine, which takes a finite difference across the central pixel in the X and Y directions to define two vectors in the slope plane and then takes their cross product to get the surface normal to that plane. These local maps are available here:

PGDA - High-Resolution LOLA Topography for Lunar South Pole Sites (https://pgda.gsfc.nasa.gov/products/78)

These slope products have stated median RMS errors of about 1.5 to 2.5 degrees. Slope derivation and error analyses are fully described in Barker et al (2021).

4.3.2 Shaded Relief Map (Hillshade)

Shaded Relief Maps, also known as Hillshade Maps, are raster images generated by modeling illumination from an artificial light source across a topographic data product. These depict surface relief using shading to emphasize changes in surface elevation using artificial light and shadows on terrain from a specified angle and altitude of the sun.

Hillshade maps can be generated from any available topographic data product using standard tools in GIS software, including commonly used software packages such as the Geospatial Data Abstraction Library, ESRI's ArcGIS, and QGIS. Hillshade maps for the lunar south pole (latitudes poleward of 87 degrees) generated from the South Pole LOLA DEM Mosaic are available here:

PGDA - South Pole LOLA DEM Mosaic (https://pgda.gsfc.nasa.gov/products/81)

This 5 m/pixel hillshade product was generated using the GDAL hillshade tool (gdaldem) with a solar incidence angle of 45 degrees from vertical and an azimuth angle of 45 degrees. Note: This is a physically unrealistic solar incidence angle for lunar polar regions but provides a good overview of local topographic relief.

For more information on illumination modeling, refer to Section 5.1.

4.3.3 Surface Roughness Analyses

Surface Roughness analyses encompass a broad array of surface characterization techniques relevant to describing the degree of variation in elevation across local scales. It is useful for understanding terrain hazards and traversability, as well as geological unit differentiation.

Surface Roughness can be estimated and reported through a variety of techniques and spatial scales. In general, surface roughness is either calculated directly from topographic data, or determined through either photometric assessment of imagery data or determined from radar data. Here, we summarize applications of various techniques.

4.3.3.1 Surface Roughness Products

Surface roughness can be estimated directly from topographic data products using a variety of techniques. The minimum spatial resolution and baseline for the roughness product is limited by the resolution of the topographic data. In general, estimates of surface roughness derived from topographic data are closely correlated with the slope determined for a terrain.

A commonly used metric to assess surface roughness is the Topographic Ruggedness Index (TRI), a measure of elevation variability between a central pixel and its neighboring eight pixels (typically using techniques similar to Horn's method). It calculates the difference in elevation values from a center cell and the eight cells immediately surrounding it. Then it squares each of the eight elevation difference values to make them all positive, sums them, and takes the square root. More information is available here:

Topographic Ruggedness Index
(https://www.usna.edu/Users/oceano/pguth/md_help/html/topo_rugged_index.htm)

4.3.3.2 Estimates from Imagery

Surface roughness can also be estimated from imagery and radar measurements, offering measurements at different spatial resolutions independent of topographically derived products. Roughness estimates can be determined in several ways:

Phase ratio observations: Planetary surfaces exhibit light backscattering and forward scattering properties based on particle size, distribution, and orientation. In other words, surface roughness affects the phase function of a material, meaning that surfaces with different roughness characteristics will scatter light differently. Ratios of images taken at different phase angles (co-registered images captured with different incident / emission angles) suppress the signal from albedo variations, emphasizing differences in roughness and related physical properties. This technique is sensitive to roughness differences at the scale of the incoming light wavelength, which in principle can enable characterization of roughness on spatial scales significantly smaller than the spatial resolution of imagery data (e.g., Kaydash et al., 2012).

Large incidence angle imagery: Imagery taken with large solar incidence angles (about 55 to 80 degrees) includes significant shadowing and shading from topographic facets. Assuming similar albedo distributions, measurements of standard deviation in pixel values correlate with surface roughness, i.e., a rougher surface will include more shadows than a smoother surface and therefore be associated with a higher standard deviation in pixel brightness. This technique estimates surface roughness at spatial scales tied to imagery data. For instance, LROC WAC images can be used as a proxy for roughness at 500 m scales, while LROC NAC images can be used as a proxy or roughness at 2.5 m scales. This technique is useful where stereo pairs and/or phase ratio observations are unavailable.

Radar Measurements: Radar instruments measuring the lunar surface detect changes in signal polarization, which can be modified by interaction of the radar wave with the lunar surface during surface reflection and subsurface scattering. The Circular Polarization Ratio (CPR) provides a quantitative measure of changes in polarization, and is strongly correlated with surface roughness at various scales, most strongly at about 100 m (e.g., Jawin et al., 2014)

4.3.4 Aspect-Slope Map

Aspect-Slope maps simultaneously show the aspect (direction) and degree (steepness) of slope for a terrain. These can be derived from any topographic product using standardized functions such as the gdaldem routines that are built into the GDAL software (https://gdal.org/programs/gdaldem.html?highlight=aspect+slope).

4.3.5 Illumination Maps

Reserved. **<TBD-ACD-50044-017>**

4.3.6 Earth Visibility Maps

Reserved. **<TBD-ACD-50044-018>**

4.3.7 Hazard Maps

Reserved. **<TBD-ACD-50044-019>**

4.4 LUNAR SURFACE GEOPHYSICAL PROPERITES

Geophysical properties are detailed in SLS-SPEC-159 Design Specifications for Natural Environments (DSNE) sections 3.4.1-3.4.2.

4.5 LUNAR SURFACE PLASMA ENVIRONMENT

The surface plasma environment is detailed in DSNE section 3.4.3.

4.6 LUNAR REGOLITH ELECTRICAL PROPERTIES

Electrical properties of the lunar regolith are listed in DSNE section 3.4.4.

4.7 LUNAR REGOLITH OPTICAL PROPERTIES

Optical properties of the lunar regolith are listed in DSNE section 3.4.5.

4.8 LUNAR THERMAL ENVIRONMENT

The thermal environment is described in DSNE section 3.4.6. **<TBD-ACD-50044-029>**

4.9 LUNAR IONIZING RADIATION ENVIRONMENT

The ionizing radiation environment is described in DSNE section 3.4.7. **<TBD-ACD-50044-030>**

4.10 LUNAR METEOROID & EJECTA ENVIRONMENT

The meteoroid and ejecta environment is described in DSNE section 3.4.8. **<TBD-ACD-50044-031>**

4.11 GEOLOGICAL MAPS

Reserved. **<TBD-ACD-50044-020> <TBD-ACD-50044-028>**

4.12 MINERALOGICAL MAPS

Reserved. **<TBD-ACD-50044-021>**

5.0 MODELING ANALYSES AND ASSUMPTIONS

Direct observational knowledge of surface features at proposed landing sites remains at the scale of meters per pixel. Every lander has a limit to the size of feature on which it can safely land. Given enough data from landing site observations and lander capability, feature measurements and lander robustness could be brought to agreement; this is shown qualitatively in Figure 5.0.1 below.

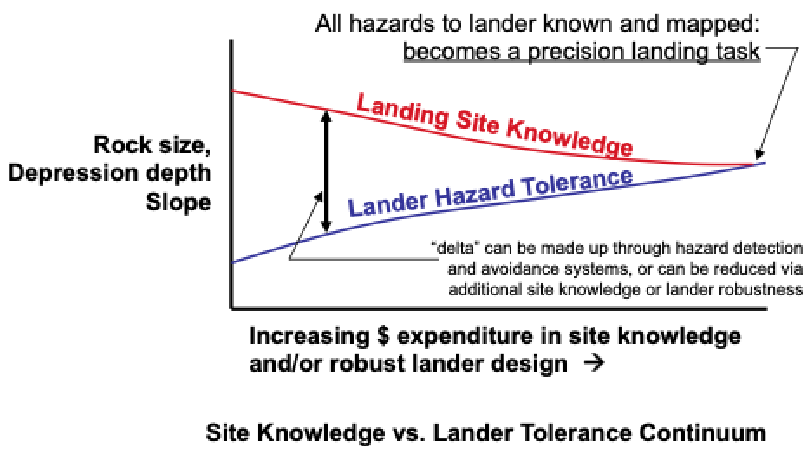

Figure 5.0.1 Site Knowledge vs. Lander Tolerance

The difference between the size of feature a lander can safely set down on and the resolution of features at the landing site can be mitigated in three ways: either the lander can be made more robust, the feature size can be further resolved, or the lander can implement hazard detection and avoidance.

The capability to process lunar surface data to a resolution that provides adequate hazard mapping varies by location on the surface. Some regions will require a lander to have a higher hazard tolerance, or higher hazard avoidance capability, than others, even with tightly-resolved feature size, due to the size of the features present. To resolve feature size, models are refined and analyzed, and assumptions are made, as described in the subsections below.

5.1 LOLA ILLUMINATION ANALYSIS

The LRO LOLA Instrument team has leveraged the LOLA dataset to simulate average illumination conditions over the 18.6-year lunar precession cycle (Mazarico et al., 2011). Illumination models leverage local topography with the orbital positions of the Earth, Moon, and Sun to derive illumination conditions across the lunar surface at a specified time or time range. These models may also consider surfaces that are illuminated through "double-bounce" photons (i.e., a surface may not experience direct illumination but may be secondarily illuminated by light reflected from local terrain). LOLA south polar models and additional background information are available here:

PGDA - Lunar Polar Illumination (https://pgda.gsfc.nasa.gov/products/69)

These models are available at 240 meters per pixel for latitudes above 65, 120 m/pixel for latitudes above 75, and 60 m/pixel for latitudes above 85. Currently, several types of illumination model are available at the PGDA link supplied above:

- **Solar Illumination:** This product indicates the percentage of model timesteps where a pixel was sunlit by any fraction of the solar disc.
- **Earth Visibility:** This product indicates the percentage of model timesteps where a pixel was lit by any fraction of the Earth disc.
- **Sky Visibility:** This product indicates the solid angle of sky not obscured by topography visible from each pixel.
- **Permanent Shadow:** This product indicates areas receiving no sunlight over the 18.6-year lunar precession cycle.

Using similar techniques, higher-resolution products (5 m/pixel) can be requested for a specified time or time range and/or elevation above the surface (please contact the SMD Artemis Spatial Data Lead, for additional information using the process in Appendix D). For example, solar illumination at 5 m above the surface of the local and surrounding terrain may be a relevant product for planning solar power arrays. More nuanced models can also be produced accounting for scattered light, percentage of visible solar/Earth disc, and/or accounting for time variability in Earthshine or solar flux.

The revised LOLA DEM products and processing methodology are described in Barker et al., (2021). More information about the derivation and properties of these models including detailed data descriptions are in the database label (LBL) files on the PDS available at:

PGDA – South Pole LOLA DEM Mosaic (https://pgda.gsfc.nasa.gov/products/81)

5.2 EARTHSHINE MAP

Earthshine is affected both by position relative to the local horizon and time-variable intensity. As defined in Glenar et al. (2019), in the context of lunar exploration, earthshine is the combined irradiance from reflected sunlight and thermal emission from Earth that illuminates the Moon. See Figure 5.2.1 for an example of an earthshine map.

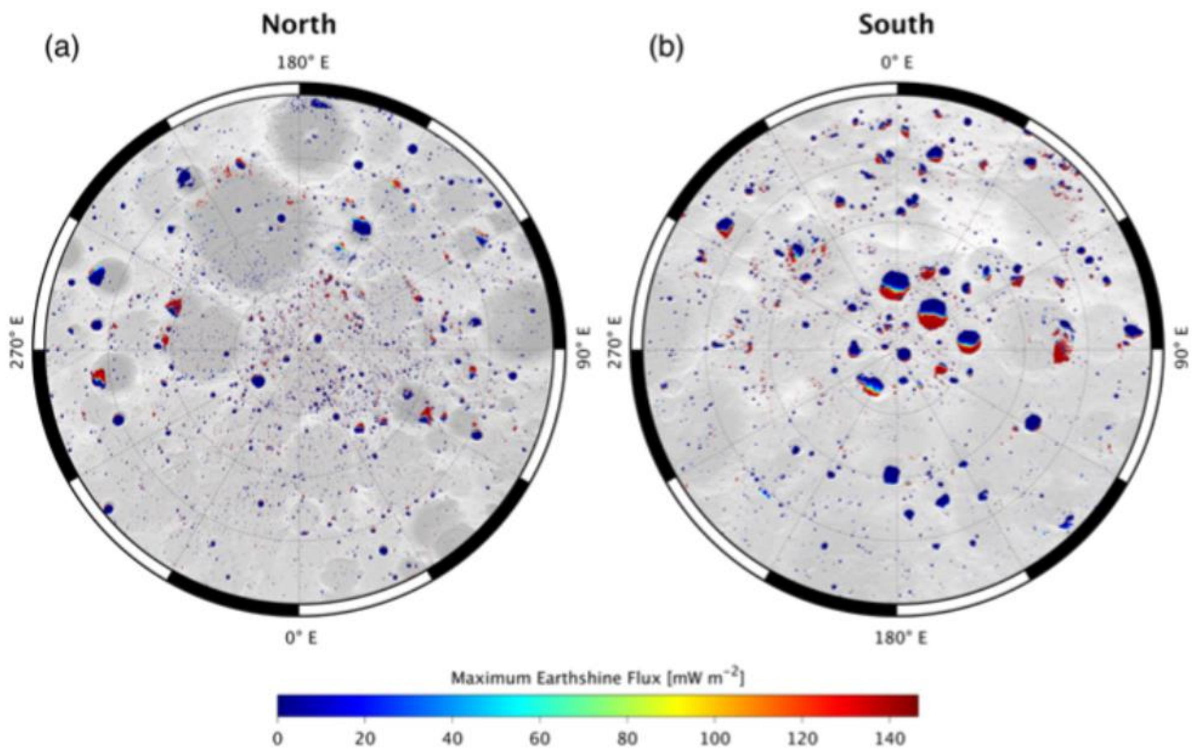

Figure 5.2.1 Maximum earthshine flux incident on lunar PSRs at the north pole (a) and south pole (b) across one 18.6-year lunar precessional cycle. Figure reproduced from Kloos & Moores (2019). The earthshine flux is overlaid on topography (grayshade).

5.3 ASSUMPTIONS

Where analytical data is not available, assumptions must be made. Common generalizations are listed here:

1. Crater diameter-to-depth ratio is 1m:10cm, or 10 cm of depth for every 1 meter of width (diameter) for craters smaller than 40m across. Larger craters are described in the DSNE, Table 3.4.1.2-1. Crater lifetimes are explored by Fassett et al (2022).

2. Boulders – referred to as "blocks" on the Moon – appear as bright, sun-facing, positive relief features; the smallest identified with confidence are 1-2 meters. Refer to Watkins et al. (2019). Lunar Surface Rock and Rock Size Distributions for > 1m rocks are defined in DSNE Section 3.4.1.4.

3. Debris size varies predictably from the rim of a crater going out from the crater, with larger blocks and more coarse debris at the rim of each impact crater, and smaller blocks and less coarse debris radiating out. (Melosh, 2011)

4. Current knowledge or data from previously explored portions of the moon will be used as assumptions when detailed information for unexplored areas is missing/unavailable.

6.0 LUNAR TERRAIN CHARACTERISTICS

6.1 GENERAL CHARACTERISTICS

The following tables describe characteristics inherent to the lunar south pole region, defined in the 2020 NASA Lunar Exploration Plan (more formally, NASA's Lunar Exploration Program Overview, https://www.nasa.gov/sites/default/files/atoms/files/artemis_plan-20200921.pdf) as the region within six degrees of latitude of the geographic lunar south pole, and are provided as a reference for vehicle design in correlation with system requirements. Global slope distribution data, that is also applicable at the south pole, is available in SLS-SPEC-159, Design Specifications for Natural Environments, for design purposes.

The lunar south pole terrain incorporates the following discrete features, in Tables 6-1 and 6-2, where (+ or -) means upslope/downslope.

Table 0.1-1 Slopes Inherent to Lunar South Pole Region

Max Slopes (°)	% South Pole Surface Area with these Slopes
0-5 (+ or -)	25%
5-10 (+ or -)	32%
10-15 (+ or -)	23%
15-20 (+ or -)	12%
20+ (+ or -)	8%

Note: Approximate areal extent of terrain with stated slopes (over a 5 m baseline) derived from the South Pole LOLA DEM Mosaic covering latitudes poleward of 87 deg. S. The derivation of this slope map is discussed in greater detail in section 4.3.1, and the DEM is described in section 4.2.2.1. The slope map was derived using Horn’s method and is available at 5 m/pixel with a stated median RMS slope error about 1.5 - 2.5°. More information on source data, slope derivation, and error estimation is available in Barker et al (2021) and here:

PGDA - South Pole LOLA DEM Mosaic (https://pgda.gsfc.nasa.gov/products/81)

PGDA - High-Resolution LOLA Topography for Lunar South Pole Sites (https://pgda.gsfc.nasa.gov/products/78)

Table 0.1-2 Lunar Regolith Trafficability Parameters

Symbol	Description	Value
n	Exponent of sinkage	1

Symbol	Description	Value
kc	Cohesive modulus	1400 N/m2
kϕ	Frictional modulus	830,000 N/m3
ϕ	Angle of internal friction	35 degrees
c	Cohesive strength of soil	170 N/m2
γ	Soil weight density	2470 N/m3
K	Coefficient of soil slip	0.018 m

Note: Tables are derived from Lunar Sourcebook (Heiken et al., 1991), which in turn was based on in-situ measurements performed by the Apollo astronauts, and the reader is referred to chapter 9 of that work for detailed information on the geotechnical properties of the lunar surface. Lunar regolith characteristics may vary, including the potential for ice mixing with regolith in/near permanently shadowed regions. For further clarification reference the Cross-Program Design Specification for Natural Environment (DSNE), SLS SPEC-159, Section 3.4.2 Lunar Regolith Properties.

6.2 CHARACTERISTICS SPECIFIC TO INTERACTION WITH THE SURFACE

Actions such as vehicles landing, rovers traversing, or crew walking change the physical characteristics of lunar regolith.

6.2.1 Plume-Surface Interaction

Vehicles that make use of rocket engines during landing, ascent, or near-surface operations create an exhaust plume that may interact with the surface beneath the vehicle. These Plume-Surface Interactions (PSI) are affected by local surface properties (e.g., regolith particle-size distribution, porosity), vehicle configuration (e.g., number and location of engines), and vehicle operations (e.g., actual descent trajectory or engine throttling). PSI may pose hazards to the lander itself, crew, and nearby assets. PSI may modify surface topography, alter the physical properties of regolith, and deposit chemical products in the vicinity of the lander. The pristine nature of the surface in the vicinity of the lander will also be affected by the PSI, which has implications for traverse planning, sampling, and the deployment of surface payloads. Use the process defined in Appendix D to request communication with the teams that model PSI.

6.2.2 Trafficability

The top layer of the lunar surface is the regolith; it ranges in thickness from meters to tens of meters and ranges in content from large rocks to microscopic particles. Lunar regolith properties including composition, particle size distribution and morphology, and geotechnical properties are defined in the DSNE Sections 3.4.2, 3.4.4, and 3.4.5. Far below the surface is the lunar crust. Figure 6.2.1 shows the lunar surface layers (Plescia, 2016):

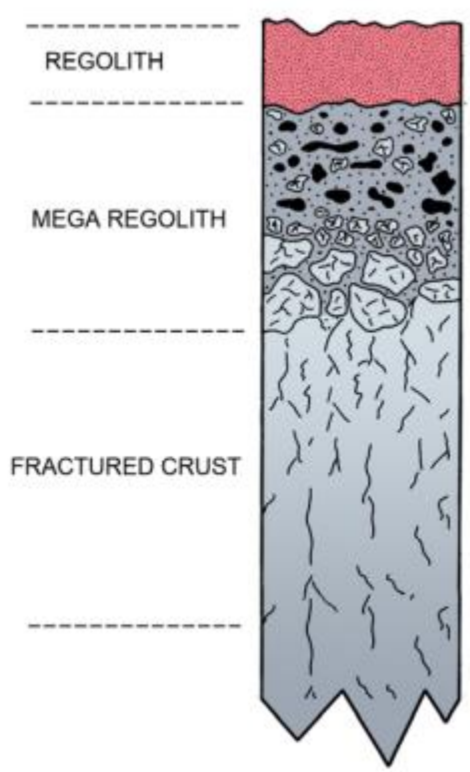

Figure 6.2.1 Lunar Surface Strata

Layers beneath and within the regolith are not uniform or universal across the surface. Impacts and thermal stress break down larger particles into smaller ones, impacts throw smaller particles out from the impact site, the heat of impact fuses smaller particles into larger ones, and the process of amalgamation bonds smaller particles together to reform larger ones again. These ongoing processes are constantly changing the surface and breaking down and remixing the composition. No single sample returned has yet been completely characterized (Plescia, 2008). The regolith in general is less compact, more deformable, more compressible, and generally less load bearing at the surface, and gets progressively more compact, less deformable, less compressible, and better able to support loads the deeper it is.

The trafficability – the ability of terrain to allow passage of vehicles or personnel – of the lunar surface varies with the size of particles in the path to be traveled and the depth of the finest particles. The low-density, uppermost layer of the regolith varies in depth and cohesion; it is less dense and deeper near the rims of young craters and more dense and shallower farther away (Plescia, 2008). The nondimensional bearing capacity of lunar soil increases as the impacting foot width goes up: wider feet (or wheels or tracks) do not sink as much as narrower ones holding the same weight. Bearing capacity as a function of footing size and the modulus of subgrade reaction are defined in DSNE section 3.4.2.4.5. Refer to Prabu et al, 2022, for an explanation of how the foot size and low gravity together impact the bear capacity of lunar soil.

Expect a path traveled by foot, wheel, or track to change over repeated use as the act of stepping on or rolling over the regolith mixes, breaks down, casts aside, and packs down that top layer.

A general overview of the characteristics of the surface presented by Dr. Plescia is available via the Lunar Planetary Institute, https://www.lpi.usra.edu/lunar/moon101/#surface (Plescia, 2008). The summary trafficability chart from that lecture is also included by Dr. Metzger in the Lunar Geology presentation, https://sciences.ucf.edu/class/wp-content/uploads/sites/23/2020/02/2020-Lunar-Geology_Metzger.pdf, where it is much more legible as slide 35 (Metzger, 2020).

<TBD-ACD-50044-038>

6.3 CHARACTERISTICS OF ILLUMINATION

Lunar south pole illumination is dependent on lunar seasons and topography. Timing of a lunar traverse must be considered with utilization objectives. For example, the lunar south pole summer provides an increased number of interconnected illuminated pathways compared to the lunar south pole winter.

On a seasonal scale, the capability of a lunar asset to survive the night/shadow will define the exploration range throughout the year. A lower tolerance to survive darkness increases limitations such as being tethered to an illuminated location, or the need to rely on an external energy source (e.g., separate utility pallet).

As an example, a lunar asset in a lunar south pole winter at Connecting Ridge, de Gerlache, Slater will experience approximately 150 continuous hours without exposure to sunlight. The derivation of the 150-hour duration is documented in Appendix E.

On the timescale of a mission, it is necessary to note that the sun moves across the sky at the rate of 12.86 degrees in 24 hours: shadows are long, sharply defined, and move extensively. The lack of atmospheric diffusion significantly minimizes light in shadows to the effects of Earthshine and solar reflection/scattering as local topography and seasonal conditions allow. Glare will be a factor any time the sun is in the field of view, in addition to bright light and deep shadow. Refer to Gläser et al, 2014.

On the timescale of a single task or EVA, it is necessary to note that the highest the sun gets above the horizon in the lunar south polar region is seven degrees. This very low angle of solar illumination means that even on the side facing the sun, there is too much light aligned to vertical surfaces, and too little light aligned to horizontal surfaces, for either cameras or human eyes to adjust to see details in both at once. Without assistance, the low angle of illumination, and the light glare and reflectance on some surfaces may affect human interaction and camera settings. Considerations for potential adaptation, shielding, etc. are suggested.

Earthshine also illuminates the surface of the Moon at the south pole from a very low angle (Metzger, 2020).

Complicating the design of task lighting, the reflectivity of lunar soil depends on the angle between the source and the observer: it reflects more light back in the direction from which it came, like a retroreflector. When looking from the same direction of the light source, details will be washed out. (Metzger, 2020). A description and visual reference for phase-dependent reflectivity can be found here on slides 16-19: https://ntrs.nasa.gov/citations/20220008695. The scattering function of light for lunar regolith is defined in DSNE Section 3.4.5.1.

<TBD-ACD-50044-032>

6.4 CHARACTERISTICS OF HAZARDS

Reserved. **<TBD-ACD-50044-022>**

7.0 EXAMPLE USE CASES LEVERAGING LUNAR SURFACE DATA

There are twenty-six distinct sites of interest identified at the lunar south pole. Figure 7.0.1 depicts these candidate landing regions. Refer to Appendix A, Table A 2-2 for more details.

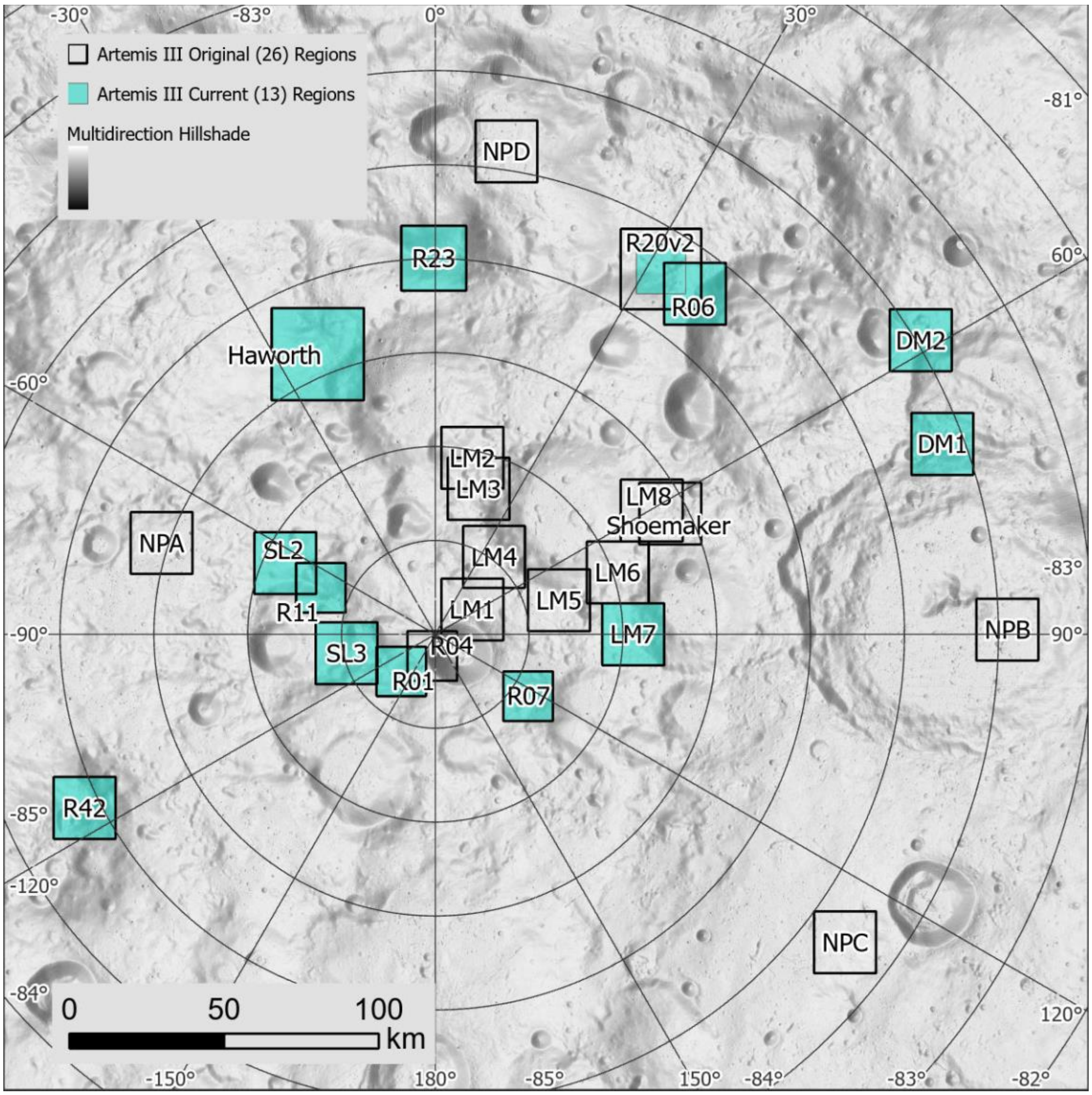

Figure 7.0.1 Candidate Landing Regions

Artemis will focus on the landmarks announced in August 2022. Figure 7.0.2 depicts the thirteen landing regions under consideration for Artemis III.

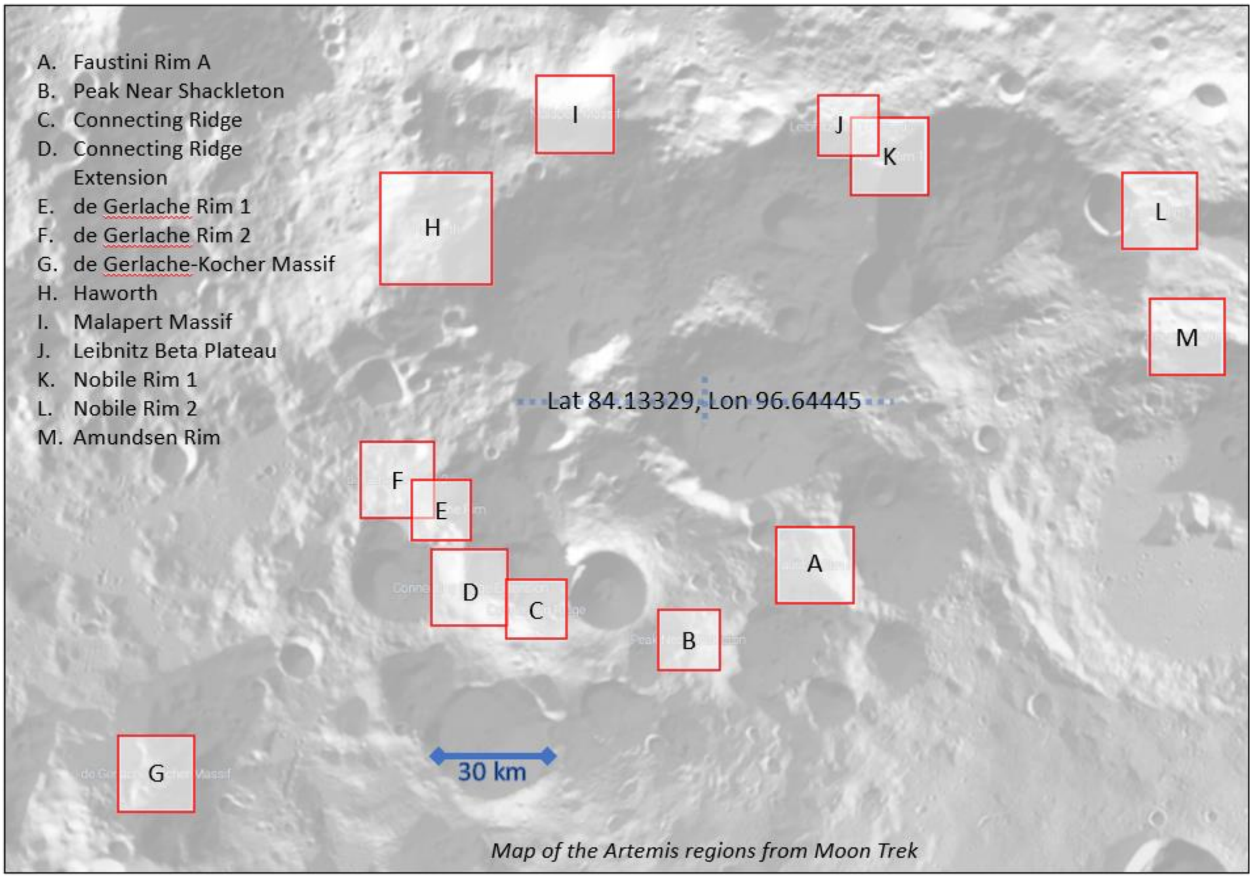

Figure 7.0.2 Artemis III Candidate Landing Regions

7.1 BASECAMP LOCATION CHARACTERISTICS

Reserved. **<TBD-ACD-50044-037>**

7.2 REPRESENTATIVE USE CASES

Representative mobility use cases are presented here to exemplify how the disparate lunar surface data sets can be used together. Table 7.2-1 presents notional categories of expected operations that mobility assets must conduct to complete the majority of the currently anticipated Artemis mission objectives. These examples do not represent definitive statements of operational mission priorities, nor do they encompass all possible exploration mobility activities on the surface of the Moon.

Table 0.2-1 Representative Use Cases

Ex.	Capability/ Traverse Type	Driving	Availability	Expected Cargo	Expected Distance	Expected Duration (Traverse Time)	Frequency (per year)
1	**Scouting and Utilization**	Hybrid*	Continuously (uncrewed and crewed mission timeframes)	Science payloads and/or small cargo	Local (**<TBD-ACD-50044-001>** range)	Varies	Frequent (many per month)
2	**Crew sortie**	Hybrid*	Crewed mission timeframes only	Science payloads, small cargo, plus crew, EVA tools	Within walk-back range (2 or 10km, **<TBR-ACD-50044-001>**)	Short (~hours)	Infrequent (~daily) during crewed missions
3**	**Large Logistics**	Hybrid*	Crewed mission timeframes only	Stressing-Heavy cargo	Local (**<TBD-ACD-50044-002>** range)	Short (~hours)	Infrequent, likely only during crewed missions
4**	**Long Uncrewed Science Traverse**	Uncrewed / teleops	Continuously during uncrewed timeframes only	Science payloads	Long (**<TBD-ACD-50044-003>** range)	Long (days or months)	Frequency **<TBD-ACD-50044-004>**
5**	**Exploring PSRs**	Hybrid*	Continuously during uncrewed timeframes only	Science payloads, with or without crew/tools	Range **<TBD-ACD-50044-005>**	Short (~hours)	Frequency **<TBD-ACD-50044-006>**
6	**Cooperative Exploration (multiple mobility assets)**	Hybrid*	Crewed mission timeframes only	Science payloads, crew, tools, cargo/logistics	Extend past walk-back range (10km, **<TBR-ACD-50044-002>**)	Potentially long cooperative traverses	Frequency (daily)
7	**<TBD-ACD-50044-033>**						

*Note: Hybrid suggests the traverse can be driven by both crewed operations and uncrewed operations (teleoperations).

**Note: Representative traverses for these use cases provided in Section 7.3.

7.3 REPRESENTATIVE TRAVERSES

The following examples represent notional, representative traverses for lunar mobility assets, and were chosen to sample the variety of conditions and demands a moving vehicle may encounter. Examples include relocation of logistics around the Artemis Base Camp (ABC) (or other fixed Artemis operating location), a long uncrewed science traverse, and a traverse into a Permanently Shadowed Region. These are example traverses only and do NOT represent definitive statements of operational mission priorities or profiles, and they do NOT encompass all possible exploration activities or destinations on the surface of the Moon.

These examples are not directly linked together unless explicitly stated. Details, acronyms, and labels in one example should not be assumed to be associated with another example. For example, PSR number labels are relevant to the figures in which they appear and are not universally recognized labels; they are not consistent across figures unless explicitly linked.

Furthermore, all traverses described here are assumed to be carried out during illuminated portions of the lunar year **<TBR-ACD-50044-003>** and subsequent planning efforts will have to account for when actual missions are planned, and thus are likely to change. Integrated technical solutions to meet the variety of terrain encountered will need to be developed with limited data. All these traverses are also described in ESDMD-410, Lunar Surface Exploration Planning: Terrain Characteristics. The purpose of this text is to provide additional context and clarifying textual information to that provided in ESDMD-410, a data managed product. Vector data files of the traverses in ESDMD-410 are available upon request; refer to Appendix D for the process by which to make a request.

7.3.1 Large Logistics Transfer

The large logistics transfer representative traverse is outlined in Example 6 of the ESDMD-410 document. This example traverse involves a logistics transfer scenario where pre-deployed supplies are transferred between two points on the Connecting Ridge between Shackleton and de Gerlache craters using a mobility asset, over a 1.3 km traverse (Figure 7.3.1). **<TBD-ACD-50044-036>**

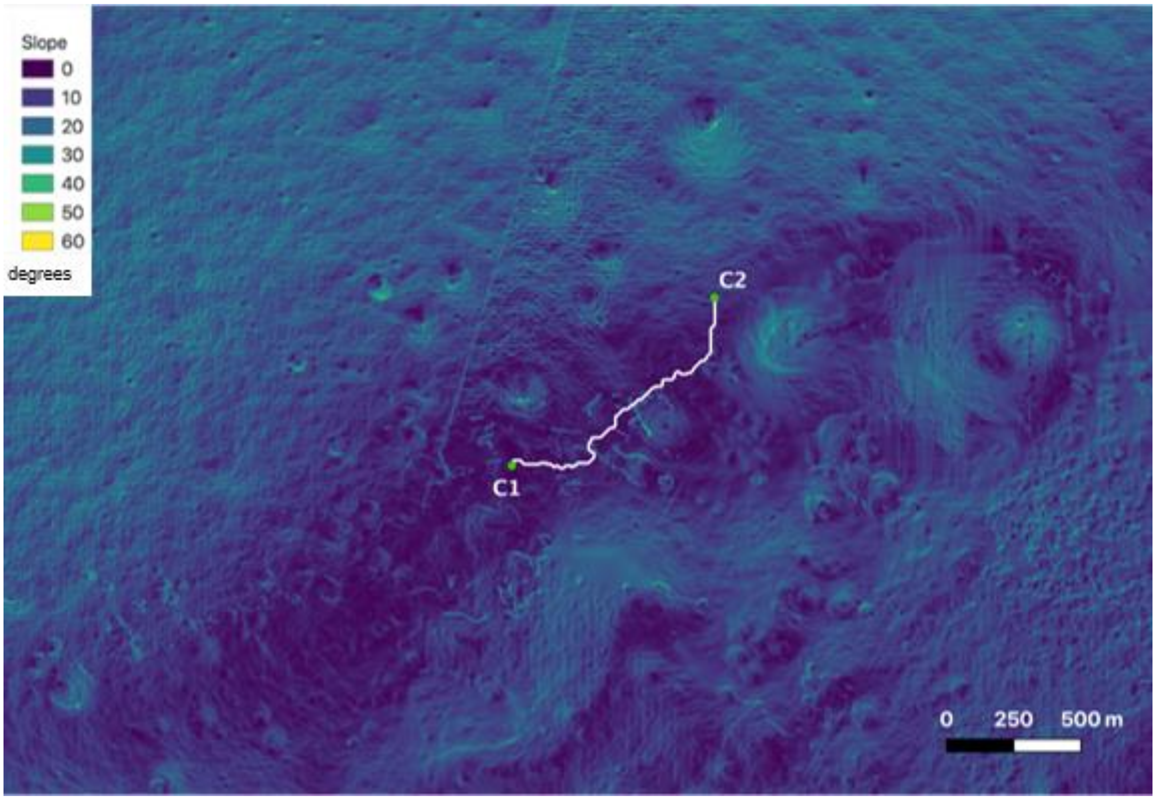

Figure 0.1 ESDMD-410 Example 6: Traverse between two points C1 (89.468° S, 222.6° E) and C2 (89.500° S, 222.1° E) on the Shackleton - de Gerlache connecting ridge. Basemap is slope information derived from USGS Astrogeology Science Center's Moon LRO South Pole DEM (https://astrogeology.usgs.gov/search/map/Moon/LRO/MOON_LRO_NAC_DEM_89S210E_4mp) using Horn (3x3) algorithm. Refer to the discussion of LOLA DEM in section 4.2.4.1.

7.3.1.1 Representative Site Terrain/Elevation Map (including PSRs)

Elevation and slope profiles are provided graphically in Figure 7.3.2. A table outlining slope statistics derived from an LROC Narrow Angle Camera Digital Elevation Model of this region is provided in Table 7.3-1. Relevant to LTV, this example traverse could include a maximum transport mass (cargo) over a shorter distance in the vicinity of fixed Artemis operating locations (known terrain), with lower speeds. Crew may be present to load/unload logistics, and the LTV may be driven by the crew during an EVA to relocate large logistics packages.

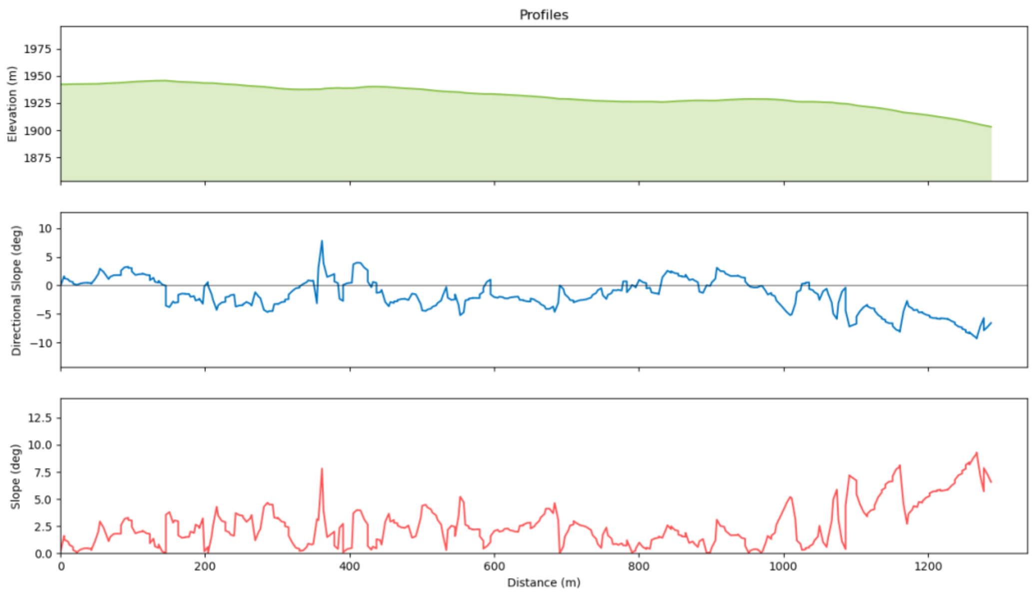

Figure 0.2 Elevation, Directional Slope, and Slope profiles for ESDMD-410 Example 6 derived from USGS Shackleton DTM.

Table 0.3-1

C1 to C2 Traverse Slope Statistics	
Minimum	0.17°
Maximum	9.76°
Mean	3.26°
Standard Deviation	1.88°

Elevation map to be added. **<TBD-ACD-50044-023>**

7.3.1.2 Representative Site Illumination

Details to be added. **<TBD-ACD-50044-023>**

7.3.1.3 Representative Site Earth Views

Details pertinent to communication to be added. **<TBD-ACD-50044-023>**

7.3.1.4 Representative Site Geological Map

Map to be added. **<TBD-ACD-50044-023> <TBD-ACD-50044-028>**

7.3.1.5 Representative Site Mineralogy and Resources

Mineralogical maps and hydrogen abundance maps to be added. **<TBD-ACD-50044-023>**

7.3.1.6 Representative Site Hazard Maps

Details of known slopes, craters, and rocks to be avoided to be added. **<TBD-ACD-50044-023>**

7.3.1.7 Representative Traverse

Most of the introductory description will be moved here, and either Figure 7.3.1 will move here or a more detailed figure will be added. **<TBD-ACD-50044-023>**

7.3.2 Long Uncrewed Science Traverse

ESDMD-410 Example 4 is a prospective uncrewed traverse using the LTV. ESDMD-410 is based on the traverse developed in Speyerer et al. 2016 (Figure 7.3.3), as a representative example to provide options for LTV utilization that enables a variety of science and prospecting use cases and maximizes movement time between Connecting Ridge (CR), Shackleton Rim (SR), and PSR points. As noted by Speyerer et al. 2016 (summarized here: http://lroc.sese.asu.edu/posts/937) this traverse does not include specific science station stops and does not assume a specific instrument suite on the vehicle; it is instead designed to maximize opportunities to achieve science and exploration objectives subject to future instrument selection and operations plan development, while keeping the vehicle illuminated for most of a calendar year. In this scenario, the vehicle lands at the site designated CR1 and the LTV may rove between CR2 and CR3 to minimize nighttime duration. The total traverse distance is 38 km, and the maximum darkness duration would be 108 hours. Traverses to SR-1, SR-2, SR-3, and into PSR-1 from the CR-1 location are feasible during illuminated periods, examples of which are provided in Figures 7.3.3 through 7.3.5. **<TBD-ACD-50044-036>**

Relevant to LTV (or any mobile asset that travels this route), this example includes representative traverses designed to avoid obviously hazardous routes **<TBD-ACD-50044-035>**, with smaller transport mass (science payloads, no crew/cargo), over relatively long distances and long durations.

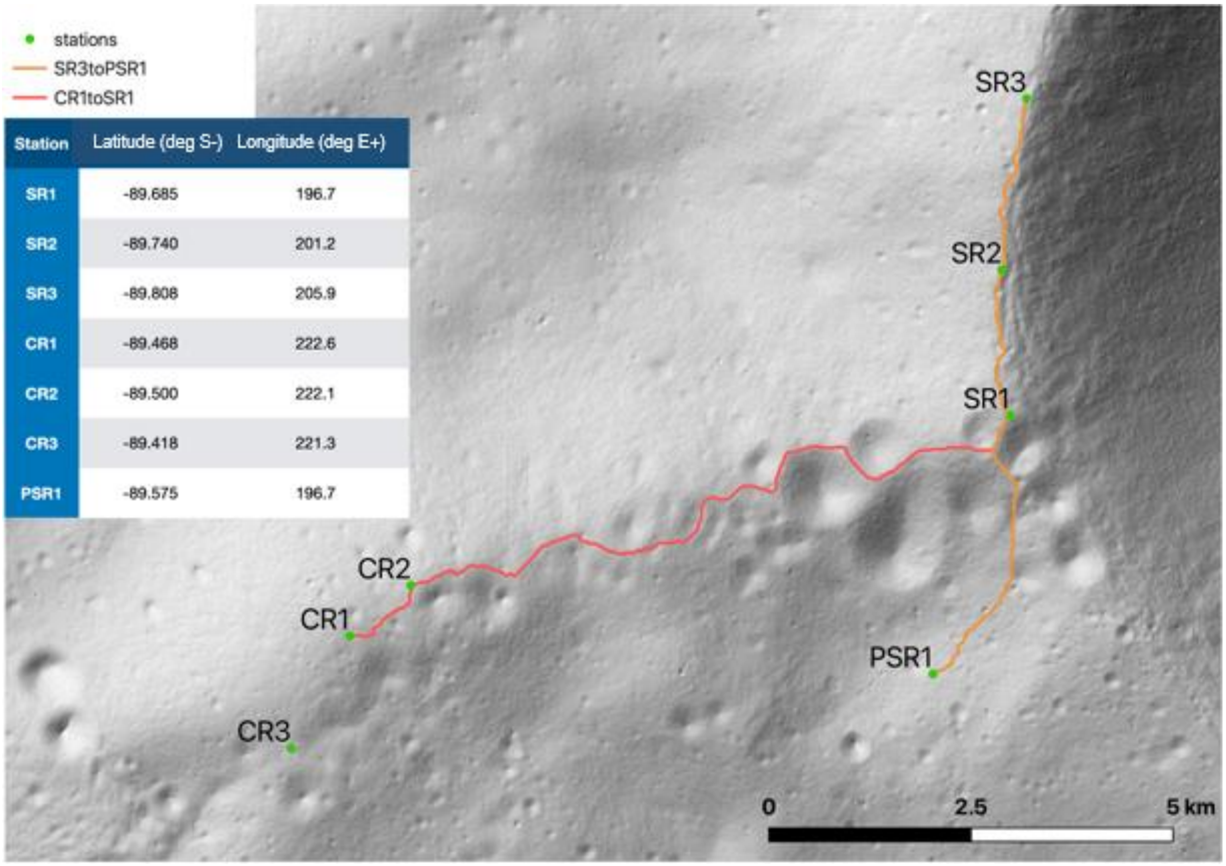

Station	Latitude (deg S-)	Longitude (deg E+)
SR1	-89.685	196.7
SR2	-89.740	201.2
SR3	-89.808	205.9
CR1	-89.468	222.6
CR2	-89.500	222.1
CR3	-89.418	221.3
PSR1	-89.575	196.7

Figure 0.3 Example of an uncrewed traverse focused on achieving science and exploration objectives and maximizing mobility in the absence of human crews, derived from Speyerer et al. 2016. Grayscale basemap is a synthetic hillshade image derived from the 5 m/pixel LOLA polar data product. Hillshade was generated with default parameters (solar azimuth: 315°; solar elevation: 45°) to quickly view terrain and thus not realistic illumination conditions.

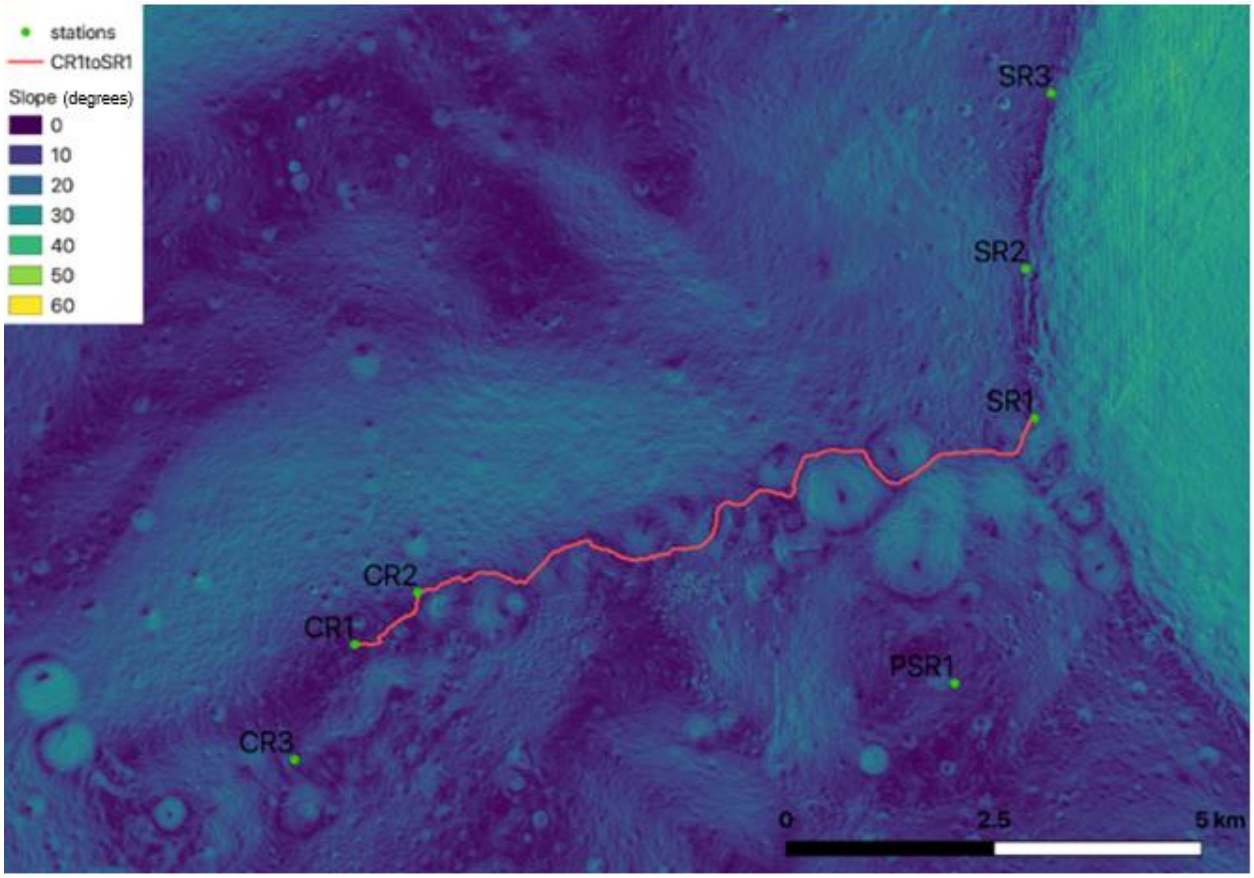

Figure 0.4 ESDMD-410 example 4 representative traverse from stations CR1 to SR1 on a slope map derived from a LROC Narrow Angle Camera Digital Elevation Model of the Shackleton - de Gerlache region.

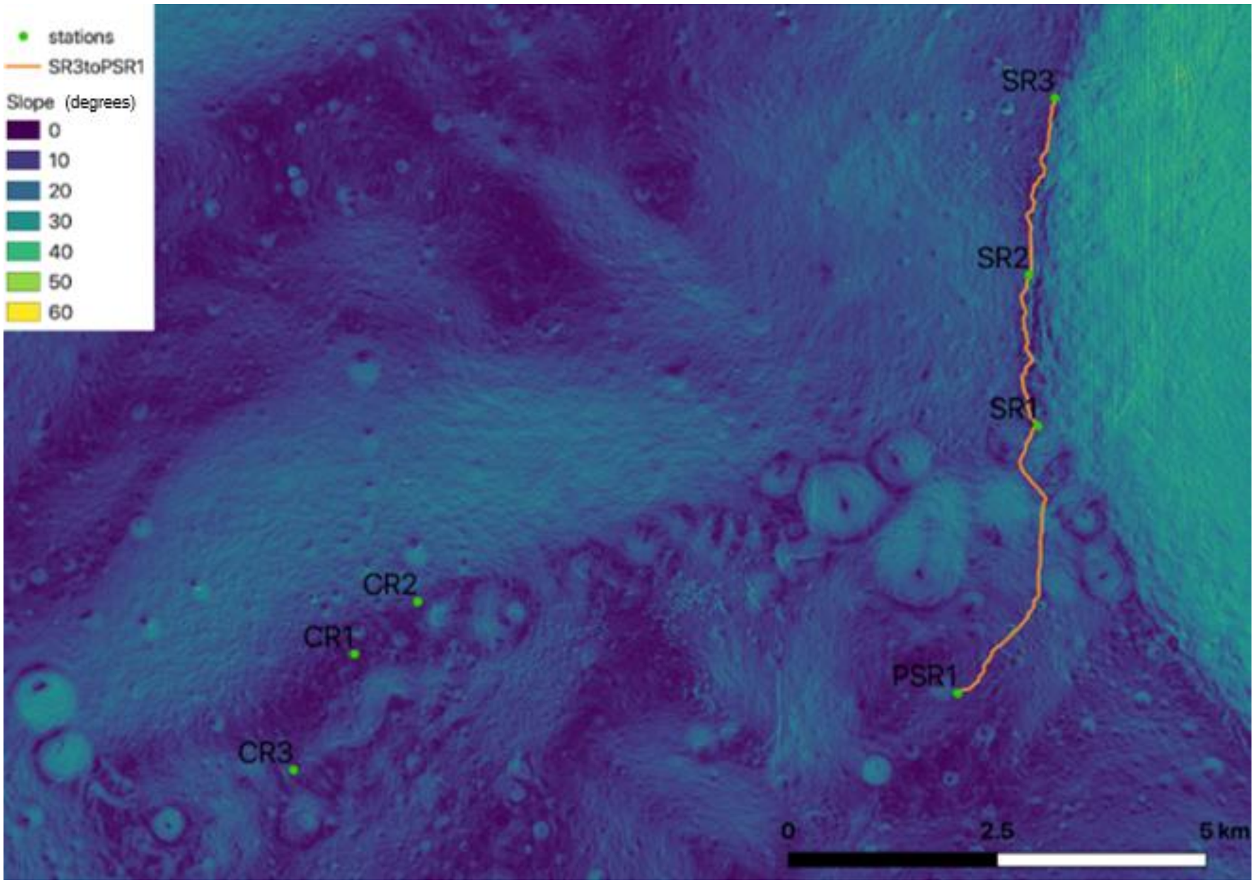

Figure 03.5 ESDMD-410 example 4 representative traverse from stations SR3 to PSR1 overlain on a slope map derived from a LROC Narrow Angle Camera Digital Elevation Model of the Shackleton - de Gerlache region.

7.3.2.1 Representative Site Terrain/Elevation Map (including PSRs)

Elevation and slope profiles are provided graphically in Figures 7.3.6 and 7.3.7; slope statistics are provided in Tables 7.3-2 and 7.3-3.

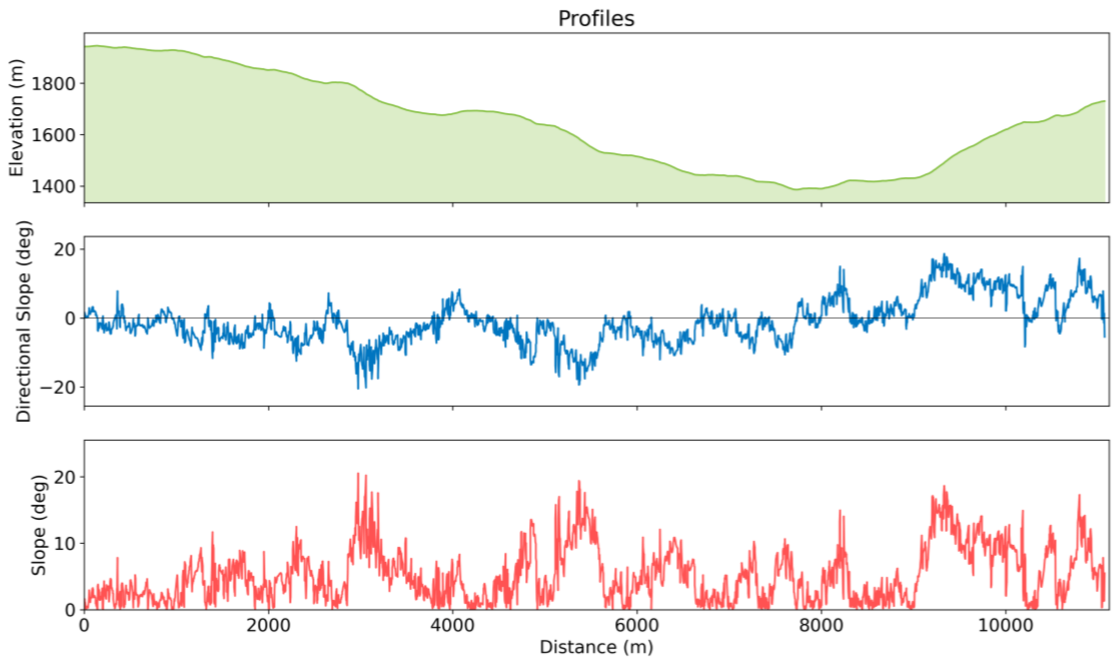

Figure 0.6 Elevation, Directional Slope, and Slope profiles for traverse path shown in Figure 7.3.4 from CR1 to SR1 extracted from a LROC Narrow Angle Camera Digital Elevation Model of the Shackleton - de Gerlache region

Table 0.3-2

CR1 to SR1 Slope Stats	
Minimum	0°
Maximum	20.51°
Mean	5.17°
Standard Deviation	4.01°

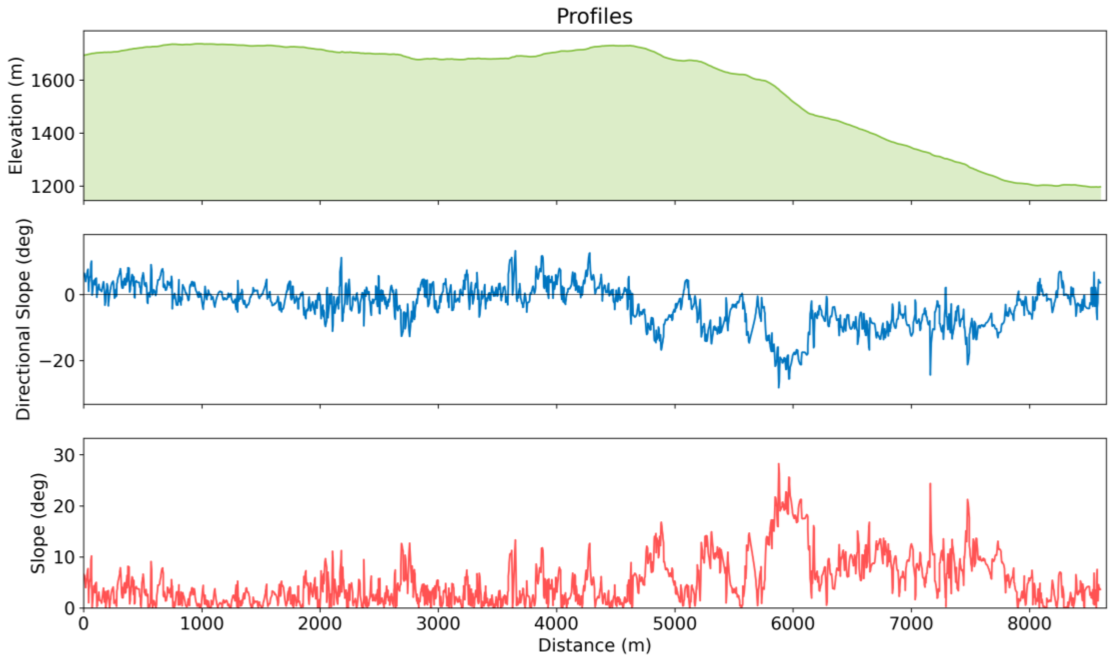

Figure 0.5 Elevation, Directional Slope, and Slope profiles for traverse path shown in Figure 7.3.5 from SR3 to PSR1 extracted from an LROC Narrow Angle Camera Digital Elevation Model of the Shackleton - de Gerlache region.

Table 0.3-3

SR3 to PSR1 Slope Statistics	
Minimum	**0°**
Maximum	**28.26°**
Mean	**5.24°**
Standard Deviation	**4.69°**

Elevation map to be added. **<TBD-ACD-50044-024>**

7.3.2.2 Representative Site Illumination

Details to be added. **<TBD-ACD-50044-024>**

7.3.2.3 Representative Site Earth Views

Details pertinent to communication to be added. **<TBD-ACD-50044-024>**

7.3.2.4 Representative Site Geological Map

Map to be added. **<TBD-ACD-50044-024> <TBD-ACD-50044-028>**

7.3.2.5 Representative Site Mineralogy and Resources

Mineralogical maps and hydrogen abundance maps to be added. **<TBD-ACD-50044-024>**

7.3.2.6 Representative Site Hazard Maps

Details of known slopes, craters, and rocks to be avoided to be added. **<TBD-ACD-50044-024>**

7.3.2.7 Representative Traverse

Most of the introductory description will be moved here, and Figures 7.3.3, 7.3.4, and 7.3.5 will move here or more detailed figures will be added. **<TBD-ACD-50044-024>**

7.3.3 Traverse into Crater/PSR

This example is based on ESDMD-410 Example 5 and provides examples of prospective crewed traverses designed to enable the exploration of cold traps near the Shackleton - de Gerlache Connecting Ridge near Spudis crater. This scenario assumes a landing at the CR1 (89.468° S, 222.6° E) location described in Section 7.3.2, from ESDMD-410 Example 4. This scenario also assumes that the surface mission increment enables at least two rover-based traverses per mission. The PSR number labels are relevant to the figures in which they appear and are not universally recognized labels. Figure 7.3.8 is the topographical map; Figure 7.3.9 shows representative elevation and slope profiles, which are summarized in Table 7.3-4. Figure 7.3.10 shows a representative round-trip traverse from CR1 to PSR3; Figure 7.3.11 shows the elevation and slope profiles, which are summarized in Table 7.3-5. Relevant to LTV (or any mobile asset that travels this route), this example traverse includes challenging terrain (steep slope), with smaller transport mass (crew and science payloads, including deployed experiments and sample collection and acquisition hardware elements), over a shorter distance than that outlined in Section 7.3.2. Crew may or may not be present, and if uncrewed, the LTV may be tele-operated from a remote-control location. **<TBD-ACD-50044-036>**

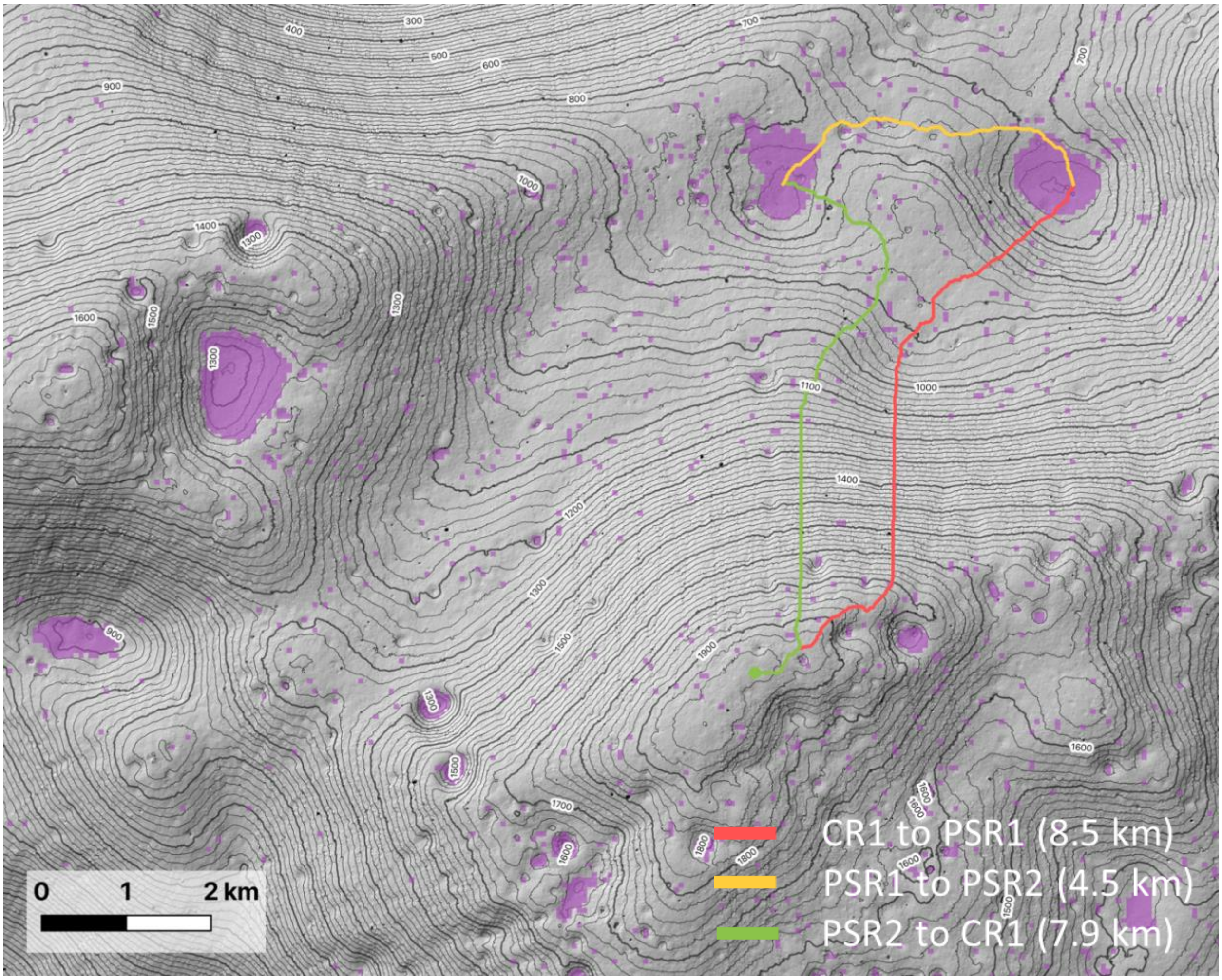

Figure 0.8 Topographic map of the Shackleton - de Gerlache Connecting Ridge, showing a round-trip traverse from CR1 to PSR1 and PSR2.

7.3.3.1 Representative Site Terrain/Elevation Map (including PSRs)

Elevation and slope profiles are provided graphically in Figures 7.3.9 and 7.3.11; slope statistics are provided in Tables 7.3-4 and 7.3-5.

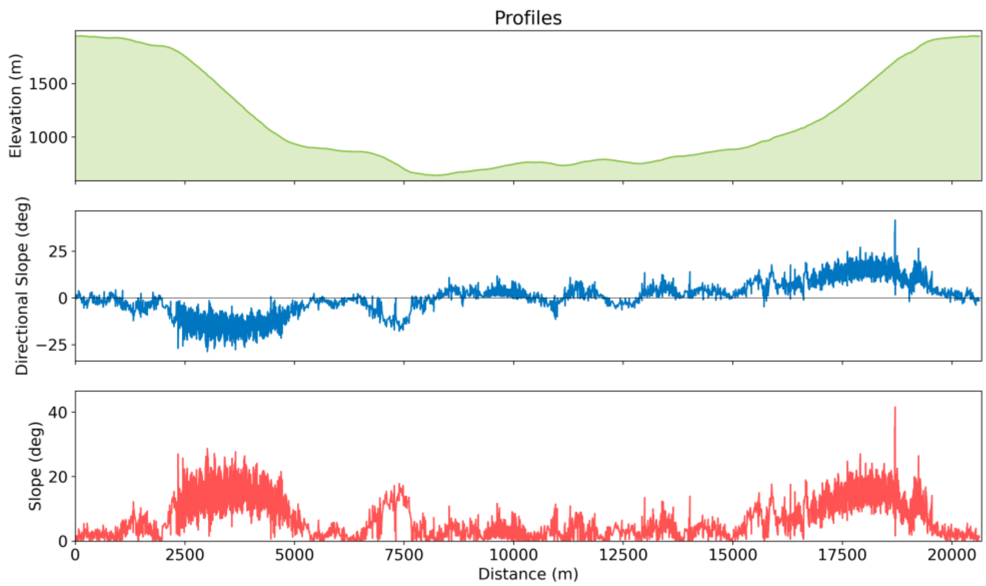

Figure 0.9 Elevation, Directional Slope, and Slope profiles for traverse path shown in Figure 7.3.8 from CR1 to PSR1 and PSR2 extracted from an LROC Narrow Angle Camera Digital Elevation Model of the Shackleton - de Gerlache region.

Table 0.3-4 Morphometry Summary of Traverse Outlined in Figure 7.3.9

Slope Stats	CR1 to PSR1	PSR1 to PSR2	PSR2 to CR1
Minimum	0.03°	0°	0°
Maximum	28.71°	11.66°	41.55°
Mean	8.4°	3.3°	7.8°
Standard Deviation	7.15°	2.03°	6.02°

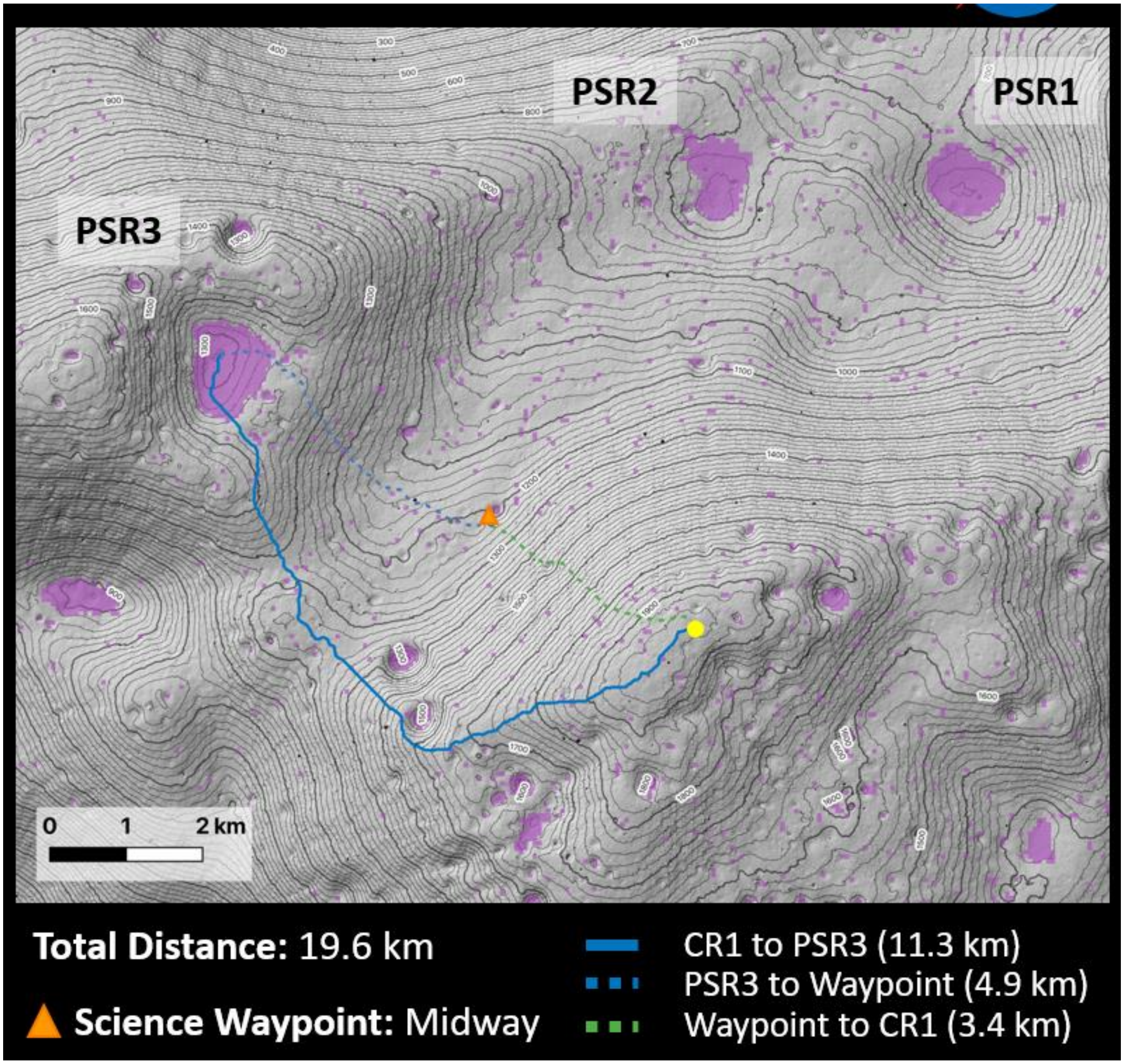

Figure 0.10 Topographic map of the Shackleton – de Gerlache Connecting Ridge showing a round-trip traverse from CR1 to PSR3.

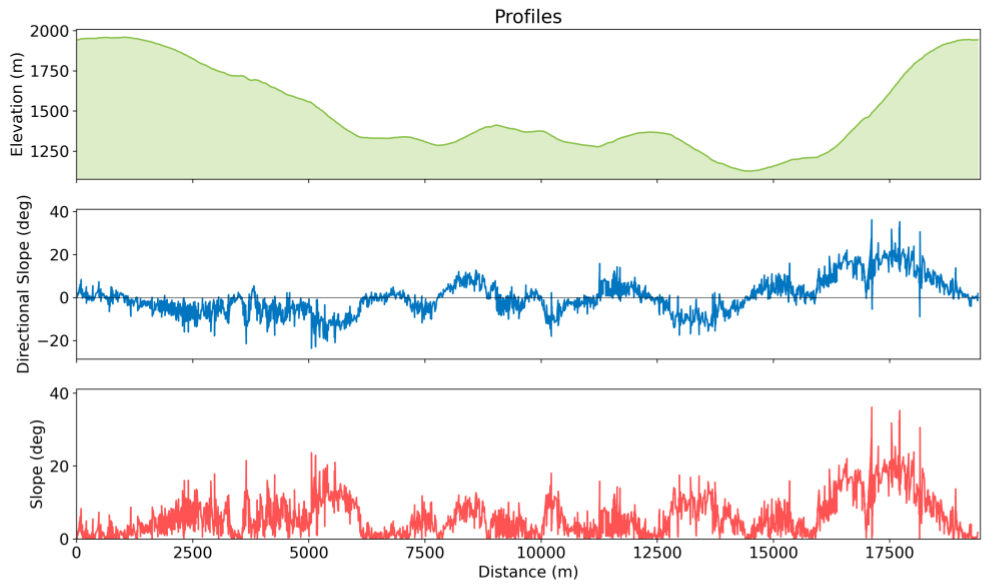

Figure 0.11 Elevation, Directional Slope, and Slope profiles for traverse path shown in Figure 7.3.10 from CR1 to PSR3 extracted from an LROC Narrow Angle Camera Digital Elevation Model of the Shackleton - de Gerlache region.

Table 0.3-5 Morphometry Summary of Traverse Outlined in 7.3.11

Slope Stats	CR1 to PSR3	PSR3 to Midway	Midway to CR1
Minimum	0°	0.02°	0°
Maximum	23.64°	17.5°	36.12°
Mean	5.28°	5°	11.65°
Standard Deviation	4.03°	3.74°	6.91°

A more detailed (easier to read) elevation map to be added. **<TBD-ACD-50044-025>**

7.3.3.2 Representative Site Illumination

Details to be added. **<TBD-ACD-50044-025>**

7.3.3.3 Representative Site Earth Views

Details pertinent to communication to be added. **<TBD-ACD-50044-025>**

7.3.3.4 Representative Site Geological Map

Map to be added. **<TBD-ACD-50044-025> <TBD-ACD-50044-028>**

7.3.3.5 Representative Site Mineralogy and Resources

Mineralogical maps and hydrogen abundance maps to be added. **<TBD-ACD-50044-025>**

7.3.3.6 Representative Site Hazard Maps

Details of known slopes, craters, and rocks to be avoided to be added. **<TBD-ACD-50044-025>**

7.3.3.7 Representative Traverse

Most of the introductory description will be moved here, and either Figure 7.3.8 and 7.3.10 will move here, or a more detailed figure will be added. **<TBD-ACD-50044-025>**

7.3.4 Crewed Science Traverse

The example in 7.3.3 above, from ESDMD-410 Example 5, also serves as a prospective crewed traverse for science mission objectives. **<TBD-ACD-50044-036>**

7.3.4.1 Representative Site Terrain/Elevation Map (including PSRs)

Elevation map to be added. **<TBD-ACD-50044-026>**

7.3.4.2 Representative Site Illumination

Details to be added. **<TBD-ACD-50044-026>**

7.3.4.3 Representative Site Earth Views

Details pertinent to communication to be added. **<TBD-ACD-50044-026>**

7.3.4.4 Representative Site Geological Map

Map to be added. **<TBD-ACD-50044-026> <TBD-ACD-50044-028>**

7.3.4.5 Representative Site Mineralogy and Resources

Mineralogical maps and hydrogen abundance maps to be added. **<TBD-ACD-50044-026>**

7.3.4.6 Representative Site Hazard Maps

Details of known slopes, craters, and rocks to be avoided to be added. **<TBD-ACD-50044-026>**

7.3.4.7 Representative Traverse

New figure. **<TBD-ACD-50044-026>**

7.3.5 Rapid Return Traverse

Also use example 7.3.3 above, from ESDMD-410 Example 5, for a stressing rapid-return traverse. **<TBD-ACD-50044-036>**

7.3.5.1 Representative Site Terrain/Elevation Map (including PSRs)

Elevation map to be added. **<TBD-ACD-50044-027>**

7.3.5.2 Representative Site Illumination

Details to be added. **<TBD-ACD-50044-027>**

7.3.5.3 Representative Site Earth Views

Details pertinent to communication to be added. **<TBD-ACD-50044-027>**

7.3.5.4 Representative Site Geological Map

Map to be added. **<TBD-ACD-50044-027> <TBD-ACD-50044-028>**

7.3.5.5 Representative Site Mineralogy and Resources

Mineralogical maps and hydrogen abundance maps to be added. **<TBD-ACD-50044-027>**

7.3.5.6 Representative Site Hazard Maps

Details of known slopes, craters, and rocks to be avoided to be added. **<TBD-ACD-50044-027>**

7.3.5.7 Representative Traverse

New figure. **<TBD-ACD-50044-027>**

APPENDIX A
ACRONYMS, ABBREVIATIONS, AND GLOSSARIES

A1.0 ACRONYMS AND ABBREVIATIONS

TABLE A1-1 ACRONYMNS AND ABBREVIATIONS

ABC	Artemis Base Camp
ACB	Artemis Campaign Development (ACD) Control Board
ACD	Artemis Campaign Development
AIAA	American Institute of Aeronautics and Astronautics
ArcGIS	(a name of a software package)
BAE	British Aerospace / Marconi Electronic Systems
CCD	Charge Coupled Device
CONOPS	Concept of Operations (may also appear as ConOps)
CPR	Circular Polarization Ratio
CR	Change Request (in reference to documents)
CR	Connecting Ridge (in reference to lunar topography)
CRaTER	Cosmic Ray Telescope for the Effects of Radiation
DEM	Digital Elevation Model
DLRE	Diviner Lunar Radiometer Experiment (usually referred to as Diviner)
DOD	Department of Defense (may also appear as DoD)
DSM	Digital Surface Model
DSNE	Design Specification for Natural Environments
DTM	Digital Terrain Model
ESA	European Space Agency
ESDMD	Exploration Systems Development Mission Directorate
ESMD	Exploration Systems Mission Directorate
ESRI	Environmental Systems Research Institute
GDAL	Geospatial Data Abstraction Library
GIS	Geospatial Information System
GRAIL	Gravity Recovery and Interior Laboratory
HEND	High Energy Neutron Detector
IJMF	International Journal of Multiphase Flow
ISIS	Integrated Software for Imagers and Spectrometers
ISRO	Indian Space Research Organisation
JAXA	Japan Aerospace eXploration Agency
JFM	Journal of Fluid Mechanics
JPL	Jet Propulsion Laboratory
LADEE	Lunar Atmosphere and Dust Environment Explorer

LAMP	Lyman Alpha Mapping Project
LBL	(a file extension)
LCROSS	Lunar Crater Observation and Sensing Satellite
LDEM	Lunar Digital Elevation Model
LEND	Lunar Exploration Neutron Detector
LEAG	Lunar Exploration Analysis Group
LIDAR	LIght Detection And Ranging
LOLA	Lunar Orbital Laser Altimeter
LRO	Lunar Reconnaissance Orbiter
LROC	Lunar Reconnaissance Orbiter Camera
LTV	Lunar Terrain Vehicle
MAPSIT	Mapping and Planetary Spatial Infrastructure Team
NAC	Narrow-Angle Camera
NASA	National Aeronautics and Space Administration
NSSDC	NASA's Space Science Data Coordinated Archive
OPR	Office of Primary Responsibility
PDS	Planetary Data System
PGDA	Planetary Geodesy Data Archive
PSI	Plume Surface Interaction
PSR	Permanently Shadowed Region
QGIS	(a name of a software package)
RF	Radio Frequency
RMS	Root Mean Square
SE&I	Systems Engineering & Integration
SfS	Shape from Shading
SLS	Space Launch System
SMD	Science Mission Directorate
SOCET SET	SOftCopy Exploitation Toolkit (a software package)
SR	Shackleton Rim
TRI	Topographic Ruggedness Index
USGS	United States Geological Survey
UV	Ultraviolet
WAC	Wide-Angle Camera

A2.0 GLOSSARY OF TERMS: LUNAR SURFACE TERMINOLOGY

The following terminology provides a common set of definition with respect to lunar terrain features that must be navigated and traversed by lunar mobility assets.

TABLE A2-1 LUNAR SURFACE TERMINOLOGY

3-Dimensional Distance	Measure of the cumulative distance along the elevation profile between two points to account for elevation gain and loss along a Euclidean or spherical distance
Artemis Base Camp (ABC)	Site(s) chosen to serve as the core initial central point and hub for near-term and long-term lunar exploration. ABC is chosen for sustained lunar missions that will involve a series of robotic and crewed missions to ensure that the terrain, lighting, and nearby lunar resources meet the long-term surface operation objectives. ABC is made up of several zones (launch and landing zone, habitation zone, power productive and utility zone, resource zones, etc.) that will require some degree of maintenance, monitoring, support a direct operation without the presence of a crew on the surface Placeholder for fixed Artemis operating locations as a group
Coordinate Reference Frame	A solution that defines from observational data the specific numerical location of given points in the reference system
Crewed	Operations performed with local crew involvement
Datum	A reference point of set of reference points on the surface against which position measurements are made
Digital Elevation Model (DEM)	A digital representation of the bare ground topographic surface of a body that excludes a natural or built surface objects
Digital Terrain Model (DTM)	A digital representation of the bare ground topographic surface of a body that excludes natural or built surface objects but does include natural/built features as vector features
Digital Surface Model (DSM)	A digital representation of the bare ground topographic surface of a body and includes natural or built surface objects
Elevation	Vertical distance of a point or object above or below a reference surface or datum
Elevation Profile	Measure of elevation gain and loss along a line between two or more points
Equatorial Circumference of Moon	10916.4 km
Euclidean Distance	Measure of the straight-line distance from one point to another in the Euclidean space in cartesian coordinates. Also known as the Pythagorean distance
Figures of Merit (FOM)	Characteristics used to quantify the relative utility of a site (or other parameter), and form a basis of comparison between multiple factors
GIS	A Geospatial Information System (GIS) is a digital system designed to capture, store, manipulate, analyze, manage, and present spatial data
Gradient	The magnitude of a slope in the steepest direction. Defined as Change in Z / Change in X. A slope relative to the LTV is described by a max slope gradient and a gradient relative to the LTV planed direction of motion or angle of attack (LTV relative slope gradient)
Hazard	Physical feature that generates a risk for the LTV and prevents its progress. *Note: Hazardous obstacles are not defined here because LTV design (traverse threshold, traverse threshold angle, etc.) will dictate which obstacles are safe or hazardous

TABLE A2-1 LUNAR SURFACE TERMINOLOGY

Height	Vertical distance above the local surface
Horn Method	An averaging method to calculate slope from eight neighboring cells/pixels about a center cell/pixel where a third-order finite difference equation is used to produce an estimate of an average slope within an 8-cell neighborhood of a central cell
Landing Ellipse	The dispersed area (either 3 sigma or 99%-tile) on the lunar surface where the is vehicle is estimated to land with the landing site at the center of the ellipse
Landing Site	A vector point data type use to indicate the exact surface location of the landing site
Lunar Digital Elevation Model (LDEM)	Topographic dataset providing an elevation (km) above fixed lunar radius of 1737.4 km
Map Points	Vector data type used to symbolize coordinates of a single object or location at the surface
Negative Obstacle	Defined by a diameter (Ø) and a negative slope. On the lunar surface they are mostly craters.
Obstacle	Physical feature that can hinder LTV progress on the lunar surface (e.g., rock, crater, slope)
Offset	Shift in datasets relative to each other due to differences in processing or data preparation
Parking Lot	Larger area that can accommodate multiple landing ellipses
Pixel	The smallest addressable element in a raster image
Positive Obstacle	Defined by a step height and a positive slope. On the lunar surface they are mostly rocks. The positive obstacle step height is the distance between the surface and the maximum height of an obstacle
Radius of Moon	1737.4 km
Raster	Data which has been processed into the form of a two-dimensional image, frequently associated with geographic data.
Region	A geographic territory that encompasses a range of features, bound together by shared characteristics, either natural or connected to the territory explored during a mission
Region of Interest	Portions of a region of expected potential scientific or other exploration value
Regolith	The surficial layer of fragmented material (rocks, soil, and dust) that covers virtually the entire surface of the Moon
Selapoid	A smooth but irregular surface whose shape results from the uneven distribution of mass within and on the surface of the Moon
Site	Location on the surface where a specific action takes place (e.g., landing, sampling, instrument deployment)
Site Plan	Similar to a terrestrial site plan, the lunar site plan is a developmental plan showing the growth of the Artemis Base Camp over time, that shows the locations, connections, and orientations of the ABC assets
Slope	Change in elevation across a certain distance (X meters)
Slope Map	A non-directional slope (degrees) at each map pixel location

TABLE A2-1 LUNAR SURFACE TERMINOLOGY

Spatial Resolution	Spatial resolution is a measure of the smallest object that can be definitively resolved by the sensor, or the ground area imaged for the instantaneous field of view (FOV) of the sensor, or the linear dimension on the ground represented by each pixel
Spherical Distance	Measure of the line that connects two points along the surface of a sphere. Also known as orthodromic distance
Terrain	Physical features of the lunar surface
Terrain Relative Navigation (TRN)	An autonomous, optical, or laser-based system for landmark recognition, spacecraft position estimation, and spacecraft retargeting
Terrain Surface Roughness	Quantified by the deviations in the direction of the normal vector of a real surface from its ideal form. The roughness is measured on a certain surface area
Traverse	Movement across the surface, either by crew or robotic assets that has a starting point and destination points and a path that connects two points
Uncrewed	Operations performed without local crew involvement
Vector	A data model that uses vertices with geographic locations to create geographic features such as points, lines, and polygons. Vector data asl may have associated spatial and non-spatial attribute data
Vehicle Footprint	The surface area bounded by the perimeter of the vehicle, with landing legs extended, on the lunar surface
Vehicle Plume Ejecta	Material that has been moved across the surface because of engine firing during descent/ascent
Zone	An area where regulations or requirements are uniform

A2.1 GLOSSARY OF TERMS: LUNAR SURFACE FEATURE NAMES

The following terminology follows that used in Mazarico et al. (2011). Coordinates have been generated from the DEM files on the PGDA website (https://pgda.gsfc.nasa.gov/products/81), so the center points of the original polygons are accurate to 5 to 10 meters.

TABLE A2-2 LUNAR SOUTH POLE FEATURES

Shorthand	Name	Latitude	Longitude
DM1	Amundsen Rim	-84.2287	69.44396
DM2	Nobile Rim 2	-83.954	58.82206
Haworth	(Haworth is its name)	-86.7639	-22.777
LM1	Shackleton Rim B	-89.5244	56.30993
LM2	Shoemaker Rim A	-88.0792	11.88866
LM3	Shoemaker Rim B	-88.3828	16.58734
LM4	Shoemaker Rim C	-88.9645	37.23483
LM5	Shoemaker Rim D	-88.632	74.62375
LM6	Shoemaker Rim E	-87.9458	71.27421
LM7	Faustini Rim A	-87.8897	90

TABLE A2-2 LUNAR SOUTH POLE FEATURES

Shorthand	**Name**	**Latitude**	**Longitude**
LM8	Shoemaker Rim F	-87.3417	60.25512
NPA	Cabeus Exterior Wall 1	-86.9243	-71.5651
NPB	Amundsen 1	-83.9046	89.53545
NPC	Idel'son L Crater 1	-84.5397	126.9045
NPD	Malapert Crater 1	-84.8034	8.387032
R01 or Site01	Connecting Ridge	-89.4632	-137.49
R04 or Site04	Shackleton Rim	-89.7668	-171.87
R06 or Site06	Nobile Rim 1	-85.4381	37.36667
R07 or Site07	Peak Near Shackleton	-88.811	123.6901
R11 or Site11	de Gerlache Rim 1	-88.6834	-67.9321
R20 or Site20	Leibnitz Beta Plateau	-85.4266	31.74276
R20v2 or Site20v2	Leibnitz Beta Plateau, extended boundaries	-85.4266	31.74276
R23 or Site23	Malapert Massif	-85.9948	-0.23578
R42 or Site42	de Gerlache-Kocher Massif	-85.8296	-116.322
Shoemaker	(Shoemaker is its name)	-87.1835	62.83502
SL2	de Gerlache Rim 2	-88.23	-64.6284
SL3	Connecting Ridge Extension	-89.0324	-101.999

APPENDIX B
REFERENCE MATERIAL

TABLE B1-1 REFERENCE SOURCES

Alexandrov, O., & Beyer, R. A. (2018). Multiview Shape-From-Shading for Planetary Images. Earth and Space Science, 5(10), 652–666. https://doi.org/10.1029/2018EA000390

Anderson, J. A., Sides, S. C., Soltesz, D. L., Sucharski, T. L., & Becker, K. J. (2004). Modernization of the Integrated Software for Imagers and Spectrometers. Abstract no. 2039. https://ui.adsabs.harvard.edu/abs/2004LPI....35.2039A

Barker, M. K., Mazarico, E., Neumann, G. A., Smith, D. E., Zuber, M. T., & Head, J. W. (2021). Improved LOLA elevation maps for south pole landing sites: Error estimates and their impact on illumination conditions. Planetary and Space Science, 203, 105119. https://doi.org/10.1016/j.pss.2020.105119

Fassett, C. I., Beyer, R. A., Deutsch, A. N., Hirabayashi, M., Leight, C. J., Mahanti, P., Nypaver, C. A., Thomson, B. J., Minton, D. A. (2022). Topographic Diffusion Revisited: Small Crater Lifetime on the Moon and Implications for Volatile Exploration. Journal of Geophysical Research: Planets, 127(12), published electronically. https://doi.org/10.1029/2022JE007510

Gladstone, G. R., Stern, S. A., Retherford, K. D., Black, R. K., Slater, D. C., Davis, M. W., Versteeg, M. H., Persson, K. B., Parker, J. W., Kaufmann, D. E., Egan, A. F., Greathouse, T. K., Feldman, P. D., Hurley, D., Pryor, W. R., & Hendrix, A. R. (2010). LAMP: The Lyman Alpha Mapping Project on NASA's Lunar Reconnaissance Orbiter Mission. Space Science Reviews, 150(1), 161–181. https://doi.org/10.1007/s11214-009-9578-6

Gläser, P., Scholten, F., De Rosa, D., Marco Figuera, R., Oberst, J., Mazarico, E., Neumann, G.A., Robinson, M.S. (2014). Illumination conditions at the lunar south pole using high resolution Digital Terrain Models from LOLA, Icarus, 243. 78–90. https://doi.org/10.1016/j.icarus.2014.08.013.

Glenar, D. A., Stubbs, T. J., Schwieterman, E. W., Robinson, T. D., Livengood, T. A. (2019) Earthshine as an illumination source at the Moon, Icarus,321, 841-856, https://doi.org/10.1016/j.icarus.2018.12.025.

Heiken, G. H., Vaniman, D. T., & French, B. M. (1991). Lunar Sourcebook, A User's Guide to the Moon. Cambridge University Press, ISBN 0-521-33444-6. https://www.lpi.usra.edu/publications/books/lunar_sourcebook/

Henriksen, M. R., Manheim, M. R., Burns, K. N., Seymour, P., Speyerer, E. J., Deran, A., Boyd, A. K., Howington-Kraus, E., Rosiek, M. R., Archinal, B. A., Robinson, M. S. (2017). Extracting accurate and precise topography from LROC narrow angle camera stereo observations, Icarus, 283, 122-137. https://doi.org/10.1016/j.icarus.2016.05.012

Jawin, E. R., Kiefer, W. S., Fassett, C. I., Bussey, B. J., Cahill, J. T. S., Dyar, M. D., Lawrence, S. J., Spudis, P. D. (2014). The relationship between radar scattering and surface roughness of lunar volcanic features. Journal of Geophysical Research: Planets, 119 (11), 2331-2348. https://doi.org/10.1002/2014JE004668

Kaydash, V., Pieters, C., Shkuratov, Y., & Korokhin, V. (2012). Lunar opposition effect as inferred from Chandrayaan-1 M^3 data. Journal of Geophysical Research: Planets, 118 (6), 1221-1232. https://doi.org/10.1002/jgre.20098

Keller, J. W., Petro, N. E., & Vondrak, R. R. (2016). The Lunar Reconnaissance Orbiter Mission – Six years of science and exploration at the Moon. Icarus, 273, 2–24. https://doi.org/10.1016/j.icarus.2015.11.024

Keszthelyi, L., Becker, T. L., Sides, S., Barrett, J., Cook, D., Lambright, S., Lee, E., Milazzo, M., Oyama, K., Richie, J., Saleh, R., Shinaman, J., Sucharscki, T., Titus, T., Walldren, J., & Weller, L. (2013). Support and Future Vision for the Integrated Software for Imagers and Spectrometers (ISIS). Abstract no. 2546. https://ui.adsabs.harvard.edu/abs/2013LPI....44.2546K/abstract

Kloos, J. L., & Moores, J. E. (2019). Mapping the Limited Extent of Earthshine within Lunar PSRs. Research Notes of the AAS, 3(9), 127. https://doi.org/10.3847/2515-5172/ab4195

Laura, J. R., & Beyer, R. A. (2021). Knowledge Inventory of Foundational Data Products in Planetary Science. The Planetary Science Journal, 2(1), 18. https://doi.org/10.3847/PSJ/abcb94

LEAG-MAPSIT, (2021). Final Report of the Lunar Critical Data Products Specific Action Team. https://doi.org/10.5281/zenodo.7236426

Mandt, K. E., Greathouse, T. K., Retherford, K. D., Gladstone, G. R., Jordan, A. P., Lemelin, M., Koeber, S. D., Bowman-Cisneros, E., Patterson, G. W., Robinson, M., Lucey, P. G., Hendrix, A. R., Hurley, D., Stickle, A. M., Pryor, W. (2016). LRO-LAMP detection of geologically young craters within lunar permanently shaded regions. Icarus 273, 114-120. https://doi.org/10.1016/j.icarus.2015.07.031

Martin, A. C., Grey, P. E., Henriksen, M. R., & Robinson, M. S. (2019). LROC NAC Feature Mosaics: An Effective Tool for Lunar Investigations. 2151, 7077. https://ui.adsabs.harvard.edu/abs/2019LPICo2151.7077M

Mazarico, E., Neumann, G. A., Smith, D. E., Zuber, M. T., Torrence, M. H. (2011). Illumination conditions of the lunar polar regions using LOLA topography. Icarus 211, 1066-1081. https://doi.org/10.1016/j.icarus.2010.10.030

Melosh, H. J. (2011) Planetary Surface Processes. Cambridge University Press, ISBN 9780511977848. https://doi.org/10.1017/CBO9780511977848

Metzger, P. (2020). Operating on the Moon: The Economic Geology of Lunar and Asteroid Resources. College of Sciences, University of Central Florida Moon 101 Course.

https://sciences.ucf.edu/class/wp-content/uploads/sites/23/2020/02/2020-Lunar-Geology_Metzger.pdf.

Mitrofanov, I.G., Bartels, A., Bobrovnitsky, Y.I. et al. (2010) Lunar Exploration Neutron Detector for the NASA Lunar Reconnaissance Orbiter. Space Sci Rev 150, 183–207. https://doi.org/10.1007/s11214-009-9608-4

Plescia, J., "'The Lunar Surface" (Moon 101 Lecture Series, The Lunar and Planetary Institute, July 16, 2008). https://www.lpi.usra.edu/lunar/moon101/#surface.

Plescia, J., "Lunar Regolith – Understanding for Science and Exploration" (LEAG Annual Meeting, November 2, 2016). https://www.hou.usra.edu/meetings/leag2016/presentations/Wednesday/plescia.pdf.

Prabu, T., Muthukkumaran, K., Venugopal, I. (2022) Study on low gravity effect on bearing capacity and slope stability of a new lunar highland soil simulant (LSS-ISAC-1) for futuristic moon habitation. Advances in Space Research, 70(7), 1869-1879. https://doi.org/10.1016/j.asr.2022.06.026.

Raney, R. K., Spudis, P. D., Bussey, B., Crusan, J., Jensen, J. R., Marinelli, W., McKerracher, P., Neish, C., Palsetia, M., Schulze, R., Sequeira, H. B., & Winters, H. (2011). The Lunar Mini-RF Radars: Hybrid Polarimetric Architecture and Initial Results. Proceedings of the IEEE, 99(5), 808–823. https://doi.org/10.1109/JPROC.2010.2084970

Robinson, M. S., Brylow, S. M., Tschimmel, M., Humm, D., Lawrence, S. J., Thomas, P. C., Denevi, B. W., Bowman-Cisneros, E., Zerr, J., Ravine, M. A., Caplinger, M. A., Ghaemi, F. T., Schaffner, J. A., Malin, M. C., Mahanti, P., Bartels, A., Anderson, J., Tran, T. N., Eliason, E. M., … Hiesinger, H. (2010). Lunar Reconnaissance Orbiter Camera (LROC) Instrument Overview. Space Science Reviews, 150(1), 81–124. https://doi.org/10.1007/s11214-010-9634-2

Sanin, A. B., Mitrofanov, I. G.,Litvak, M. L., Bakhtin, B.N., Bodnarik, J. G., Boynton, W. V., Chin, G., Evans, L. G., Harshman, K., Fedosov, F., Golovin, D. V., Kozyrev, A. S., Livengood, T. A., Malakhov, A. V., McClanahan, T. P., Mokrousov, M. I., Starr, R. D., Sagdeev, R. Z., Tret'yakov, V. I., Vostrukhin, A. A. (2017). Hydrogen distribution in the lunar polar regions. Icarus, 283, 20-30. https://doi.org/10.1016/j.icarus.2016.06.002

Smith, D. E., Zuber, M. T., Neumann, G. A., Lemoine, F. G., Mazarico, E., Torrence, M. H., McGarry, J. F., Rowlands, D. D., Head III, J. W., Duxbury, T. H., Aharonson, O., Lucey, P. G., Robinson, M. S., Barnouin, O. S., Cavanaugh, J. F., Sun, X., Liiva, P., Mao, D., Smith, J. C., & Bartels, A. E. (2010). Initial observations from the Lunar Orbiter Laser Altimeter (LOLA). Geophysical Research Letters, 37(18). https://doi.org/10.1029/2010GL043751

Spence, H. E., Case, A. W., Golightly, M. J., Heine, T., Larsen, B. A., Blake, J. B., Caranza, P., Crain, W. R., George, J., Lalic, M., Lin, A., Looper, M. D., Mazur, J. E., Salvaggio, D., Kasper, J. C., Stubbs, T. J., Doucette, M., Ford, P., Foster, R., … Charara, Y. (2010). CRaTER: The Cosmic Ray Telescope for the Effects of Radiation Experiment on the

Lunar Reconnaissance Orbiter Mission. Space Science Reviews, 150(1), 243–284. https://doi.org/10.1007/s11214-009-9584-8

Speyerer, E. J., Lawrence, S. J., Stopar, J. D., Gläser, P., Robinson, M. S., & Jolliff, B. L. (2016). Optimized traverse planning for future polar prospectors based on lunar topography. Icarus, 273, 337–345. https://doi.org/10.1016/j.icarus.2016.03.011

Stickle, A., & Stoper, J. (2021). Final Report of the Lunar Critical Data Products Specific Action Team. Lunar Exploration Analysis Group (LEAG). https://doi.org/10.5281/zenodo.7236426

Vondrak, R., Keller, J., Chin, G., & Garvin, J. (2010). Lunar Reconnaissance Orbiter (LRO): Observations for Lunar Exploration and Science. Space Science Reviews, 150(1), 7–22. https://doi.org/10.1007/s11214-010-9631-5

Watkins, R. N., Jolliff, B. L., Mistick, K., Fogerty, C., Lawrence, S. J., Singer, K. N., Ghent, R. R. (2019). Boulder Distributions Around Young, Small Lunar Impact Craters and Implications for Regolith Production Rates and Landing Site Safety. Journal of Geophysical Research: Planets, 124(11), 2754-2771. https://doi.org/10.1029/2019JE005963

Williams, J.-P., Greenhagen, B. T., Paige, D. A., Schorghofer, N., Sefton-Nash, E., Hayne, P. O., Lucey, P. G., Siegler, M. A., & Aye, K. M. (2019). Seasonal Polar Temperatures on the Moon. Journal of Geophysical Research: Planets, 124(10), 2505–2521. https://doi.org/10.1029/2019JE006028

TABLE B1-2 ADDITIONAL REFERENCES NOT CITED IN TEXT

Balakrishnan, K., & Bellan, J. (2018). High-Fidelity Modeling and Numerical Simulation of Cratering Induced by the Interaction of a Supersonic Jet with Granular Soil. International Journal of Multiphase Flow, 99(2), 1-29. https://doi.org/10.1016/j.ijmultiphaseflow.2017.08.008

Balakrishnan, K., & Bellan, J. (2019). A Multi-Species Modeling Framework for Describing Supersonic-Jet Induced Cratering in a Granular Bed: Cratering on Titan Case Study. International Journal of Multiphase Flow, 118, 205–241, 2019. https://doi.org/10.1016/j.ijmultiphaseflow.2019.05.011

Balakrishnan, K., & Bellan, J. (2021). Fluid density effects in supersonic jet-induced cratering in a granular bed on a planetary body having an atmosphere in the continuum regime. Journal of Fluid Mechanics, 915, A29. https://doi.org/10.1017/jfm.2021.29

Balakrishnan, K., & Bellan, J. (2021). Ejecta Formed During Supersonic Jet-induced Cratering in a Granular Medium.), AIAA Journal, 59(10), 3799-3814. https://doi.org/10.2514/1.J060563

Balakrishnan, K., & Bellan, J. (2023). Added Mass and Pseudo-Turbulent Kinetic Energy Effects on Ejecta during Jet-Induced Cratering in a Soil. AIAA Journal, 63(3), 973-990. https://doi.org/10.2514/1.J062405

Fontenot, R.L., Talbot, J., Gale, M., Mehta, R.S., and Capecelatro, J. (2022) “Modeling Enhancements for Eulerian-Eulerian Two-Fluid Methods in Compressible Particle-Laden Flows with Plume-Surface Interaction Applications,” Paper 2022-2195, AIAA SciTech 2022 Forum, San Diego, CA, January 2022. https://arc.aiaa.org/doi/abs/10.2514/6.2022-2195

Gale, M. (2022) “Efficient Pseudo-Polydisperse Model for Plume-Surface Interaction in Spacecraft Propulsive Landings,” AIAA Paper 2022-2002, AIAA SciTech 2022 Forum, San Diego, CA, January 2022. https://arc.aiaa.org/doi/pdf/10.2514/6.2022-2002

Gale, M., and Harris, R. (2022) “Continuum-Rarefied Modeling of Plume-Surface Interaction in Low-Pressure Environments,” AIAA Paper 2022-2003, AIAA SciTech 2022 Forum, San Diego, CA, January 2022. https://arc.aiaa.org/doi/abs/10.2514/6.2022-2003

Gale, M., Mehta, R.S., Liever, P., Curtis, J., and Yang, J. (2020) “Realistic Regolith Models for Plume-Surface Interaction in Spacecraft Propulsive Landings,” AIAA Paper 2020-0797, AIAA SciTech 2020 Forum, January 2020. https://arc.aiaa.org/doi/10.2514/6.2020-0797

Howison, J.C., Gale, M., and Mehta, R.S. (2022) “An Automated Process to Generate Constitutive Models for Granular Mixtures Using LIGGGHTS,” Paper 2022-2194, AIAA SciTech 2022 Forum, San Diego, CA, January 2022. https://arc.aiaa.org/doi/10.2514/6.2022-2194

Liever, P.A, Gale, M.P., Mehta, R.S., Weaver, A.B., West, J.S., Westra, D.G. (2021) “Gas-Particle Flow Simulations for Martian and Lunar Lander Plume-Surface Interaction Prediction,” ASCE Earth and Space 2021 Conference, April 2021. https://ascelibrary.org/doi/10.1061/9780784483374.009

Liever, P.A., and West, J.S. (2021) “Advances in Plume-Surface Interaction Simulation Capability Under Lunar Landing Conditions,” International Planetary Probe Workshop, August 2021. https://youtu.be/KpSRkOFEszg

Liever, P., and West, J. (2022) “Particle Interaction Physics Model Formulation for Plume-Surface Interaction Erosion and Cratering,” Paper 2022-2317, AIAA SciTech 2022 Forum, San Diego, CA, January 2022. http://dx.doi.org/10.2514/6.2022-2317

Liever, P., and West, J. (2022) “Demonstration of Capability to Simulate Particle Irregular Shape and Poly-Disperse Mixtures Within Lunar Lander Plume-Surface Interaction,” ASCE Earth and Space 2022 Conference, April 2022. https://ascelibrary.org/doi/10.1061/9780784484470.006

Shurtz, T.P., Krolick, W., Weaver, A.B., and West, J. (2022) “A Hybrid CFD/Engineering Model for Predicting Plume Induced Erosion and Cratering,” 19th International Planetary Probe Workshop, Santa Clara, CA, September 2022. https://drive.google.com/file/d/1FBbKn9HovFDO-5cqDYJVZjz6dIm5TVPB/view

Shurtz, T., Liever, P., Weaver, A., and West, J. (2020) “Flow Simulations for Martian and Lunar Lander Plume-Surface Interaction Prediction,” NASA In-Space Chemical Propulsion TIM, Huntsville, AL, September 2020. https://ntrs.nasa.gov/citations/20205004634

Weaver, A.B., Krolick, W.C., Liever, P.A., and West, J.S. (2022) “Overview of Predictive Simulation Capability Development for Crater Evolution and Ejecta in Continuum/Rarefied Flows,” Paper 2022-2320, AIAA SciTech 2022 Forum, San Diego, CA, January 2022. https://arc.aiaa.org/doi/abs/10.2514/6.2022-2320

West, J. S., and Liever, P.A. (2022) “Gas-Particle Interaction Model Development in Plume Surface Interaction Erosion and Cratering,” Paper 2022-2321, AIAA SciTech 2022 Forum, San Diego, CA, January 2022. https://arc.aiaa.org/doi/abs/10.2514/6.2022-2321

West, J.S., Liever, P., Weaver, A., Shurtz, T.P., Gale, M., Krolick, W. C., and Griffin, L.W. (2022) “Overview of the Predictive Simulation Capability Element of the Plume Surface Interaction Project,” Paper 2022-2319, AIAA SciTech 2022 Forum, San Diego, CA, January 2022. https://arc.aiaa.org/doi/10.2514/6.2022-2319

TABLE B1-3 REFERNCE LINK SHORTHAND

Short Name	Description of Reference	Link
	<TBD-ACD-50044-034>	

APPENDIX C OPEN WORK

C1.0 TO BE DETERMINED

The table To Be Determined Items lists the specific items in the document that are not yet known. The TBD is inserted as a placeholder wherever the required data is needed and is formatted in bold type within carets. The TBD item is numbered based on the document number (i.e., **<TBD-xxxx-00x-00x>** is the first undetermined item assigned in the document). As each TBD item is resolved, the updated text is inserted in each place that the TBD appears in the document and the item is removed from this table. As new TBD items are assigned, they will be added to this list in accordance with the above-described numbering scheme. Original TBD items will not be renumbered.

TABLE C1-1 TO BE DETERMINED ITEMS

TBD	Section	Description
TBD-ACD-50044-001	7.2	Range for Scouting and Utilization Traverse
TBD-ACD-50044-002	7.2	Range for Large Logistics Traverse
TBD-ACD-50044-003	7.2	Range for Long Uncrewed Science Traverse
TBD-ACD-50044-004	7.2	Frequency of Long Uncrewed Science Traverse
TBD-ACD-50044-005	7.2	Range for Exploring PSRs Traverse
TBD-ACD-50044-006	7.2	Frequency of Exploring PSRs Traverse
TBD-ACD-50044-007 CLOSED	6.3	Reference for 150-hr period of darkness – expecting content for a new appendix -:- CLOSED by Revision A, Appendix E -:-
TBD-ACD-50044-008	3.1.1	Discussion of Apollo data
TBD-ACD-50044-009	3.1.2	Discussion of Lunokhod data
TBD-ACD-50044-010	3.2.2	Discussion of Clementine data
TBD-ACD-50044-011	3.2.3	Discussion of Lunar Prospector data
TBD-ACD-50044-012	3.2.4	Discussion of Kaguya data
TBD-ACD-50044-013	3.2.5	Discussion of LCROSS data
TBD-ACD-50044-014	3.2.6	Discussion of GRAIL data
TBD-ACD-50044-015	3.2.7	Discussion of Chandrayan data
TBD-ACD-50044-016	3.2.8	Discussion of Danuri data
TBD-ACD-50044-017	4.3.5	Provide general illumination maps (by inclusion or link)
TBD-ACD-50044-018	4.3.6	Provide general earth visibility maps (by inclusion or link)
TBD-ACD-50044-019	4.3.7	Provide general hazard maps (by inclusion or link)

TBD	Section	Description
TBD-ACD-50044-020	4.11	Provide general geological maps (by inclusion or link)
TBD-ACD-50044-021	4.12	Provide general mineralogical maps (by inclusion or link)
TBD-ACD-50044-022	6.4	Discussion of general hazard characteristics created by the terrain, including dust, solar wind, plasma, and potential voltage differences in PSRs
TBD-ACD-50044-023	7.3.1	Add details to the Large Logistics Transfer Traverse data presentation – not all the subsections associated with this TBD may be used, after the general maps are added by earlier-occurring TBDs
TBD-ACD-50044-024	7.3.2	Add details to the Long Uncrewed Science Traverse data presentation – not all the subsections associated with this TBD may be used, after the general maps are added by earlier-occurring TBDs
TBD-ACD-50044-025	7.3.3	Add details to the Traverse into Crater data presentation – not all the subsections associated with this TBD may be used, after the general maps are added by earlier-occurring TBDs
TBD-ACD-50044-026	7.3.4	Add details to the Crewed Science Travers data presentation – not all the subsections associated with this TBD may be used, after the general maps are added by earlier-occurring TBDs
TBD-ACD-50044-027	7.3.5	Add details to the Rapid Return Traverse data presentation – not all the subsections associated with this TBD may be used, after the general maps are added by earlier-occurring TBDs
TBD-ACD-50044-028	4.11 & 7.3	Discuss the accuracy, resolution, and any smoothing of elevation & slope data. Include error bars if possible.
TBD-ACD-50044-029	4.8	Provide detailed thermal discussion and context for use of DSNE 3.4.6.2 through 3.4.6.4
TBD-ACD-50044-030	4.9	Provide detailed radiation discussion and context for use of DSNE 3.4.7
TBD-ACD-50044-031	4.10	Provide detailed ejecta and micrometeoroid discussion and context for use of DSNE 3.4.8
TBD-ACD-50044-032	6.3	Discuss aspects of illumination, including reflectance, irradiance, and spectrum details; address how much continuous illumination can be expected after 150 hours of darkness

TBD	Section	Description
TBD-ACD-50044-033	7.2	Add example use cases for small logistics or utility pallet, and other asset types (including PR and CLPS as deemed appropriate)
TBD-ACD-50044-034	Appendix B	Table B1-3 to organize the links in the document, give them all short names, acknowledge data collections as such (as opposed to data from individual sources), and allow their long form to be collected in one place and removed from the prose
TBD-ACD-50044-035	7.3.2	Describe how obviously hazardous routes are identified; likely related to section 6.4 and TBD-ACD-50044-022
TBD-ACD-50044-036	7.3.1, 7.3.2, 7.3.3, 7.3.4, 7.3.5	Describe how each example traverse path was chosen (why the start/finish points, why the route, how is it unique, etc.)
TBD-ACD-50044-037	7.1	Discuss desired and expected characteristics of the candidate base camp locations
TBD-ACD-50044-038	6.2	Discuss whether or not, or in what condition it is or is not, advantageous to travel the same path or land at the same location repeatedly

C2.0 TO BE RESOLVED

The table To Be Resolved Items lists the specific items in the document that are not yet officially baselined. The TBR is inserted as a placeholder wherever the listed data is unofficial and is formatted in bold type within carets. The TBR item is numbered based on the document number (i.e., **<TBR-xxxx-00x-00x>** is the first unresolved item assigned in the document). As each TBR item is resolved, the updated text is inserted in each place that the TBR appears in the document and the item is removed from this table. As new TBR items are assigned, they will be added to this list in accordance with the above-described numbering scheme. Original TBR items will not be renumbered.

TABLE C2-1 TO BE RESOLVED ITEMS

TBR	Section	Description
TBR-ACD-50044-001	7.2	Walk-back Range of Crew Sortie Traverse
TBR-ACD-50044-002	7.2	Extend Past Walk-back Range for Cooperative Exploration Traverse
TBR-ACD-50044-003	7.3	Clarify “illuminated portions of the calendar year” and other timing limitations addressed or specifically ignored for each traverse

APPENDIX D DATA REQUEST PROCESS

D1.0 OVERVIEW OF THE DATA REQUEST PROCESS

Write a brief statement with the requestor's name, the data needed, the need-by-date, names and email addresses of other parties to be included on additional communication, and the purpose/program for which the requested data will be used.

D1.1 HOW TO INITIATE A FORMAL DATA REQUEST

To request existing data as listed in this data book or to request a new data product from the Artemis Geospatial Data Team, send the statement via electronic mail to JSC-ArtemisGeospatialTeam@mail.nasa.gov.

D1.2 HOW A FORMAL DATA REQUEST WILL BE PROCESSED

The statement will be reviewed and forwarded to the appropriate data representative for further collaboration with the requestor. Please allow ten business days for initial processing; clarification may be sought by reply to the sending address and the listed other parties.

APPENDIX E 150 HOURS OF DARKNESS

E1.0 "SURVIVE THE NIGHT"

The typical lunar night duration is approximately 14 days with the lunar poles experiencing extremes in illumination such as permanently shadowed regions within craters or areas with increased lighting duration on crater rims or ridges during the lunar summer season. The duration of light and shadow are influenced by location, elevation, and season. Figure E.1 shows a map of the solar illumination, averaged over hourly timesteps spanning 18.6 years, for the lunar south pole region from 85°S-90°S (E.Mazarico, PGDA - Lunar Polar Illumination (nasa.gov))

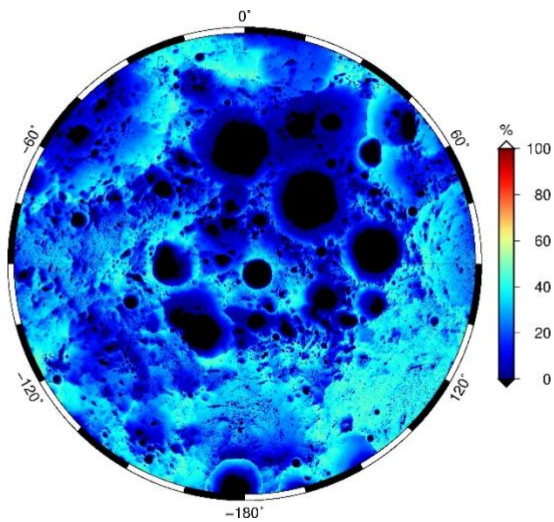

Figure E.1 Map of the solar illumination, averaged over hourly timesteps spanning 18.6 years, for the south polar region, 85S-90S (center, 60m/px)

Using an initial lighting analysis of the Connecting Ridge location as an example, results show there is no site with 100% illumination on the Connecting Ridge. A minimum shadow duration of 85 hours will be needed to complete a shorter traverse, ~10 km in distance, on the Connecting Ridge.

Figures E.2 shows an example, longer traverse path between Connecting Ridge and de Gerlache displayed as an path illumination matrix (distance vs time) and stereographic plots on specific days (E.Mazarico, Sunlit pathways between south pole sites of interest for lunar exploration - ScienceDirect). Planning this ~55km traverse involves finding a path that prioritizes illumination (represented as yellow or white) and minimizes periods of darkness (represented as blue or black) resulting in a ~30 day trip.

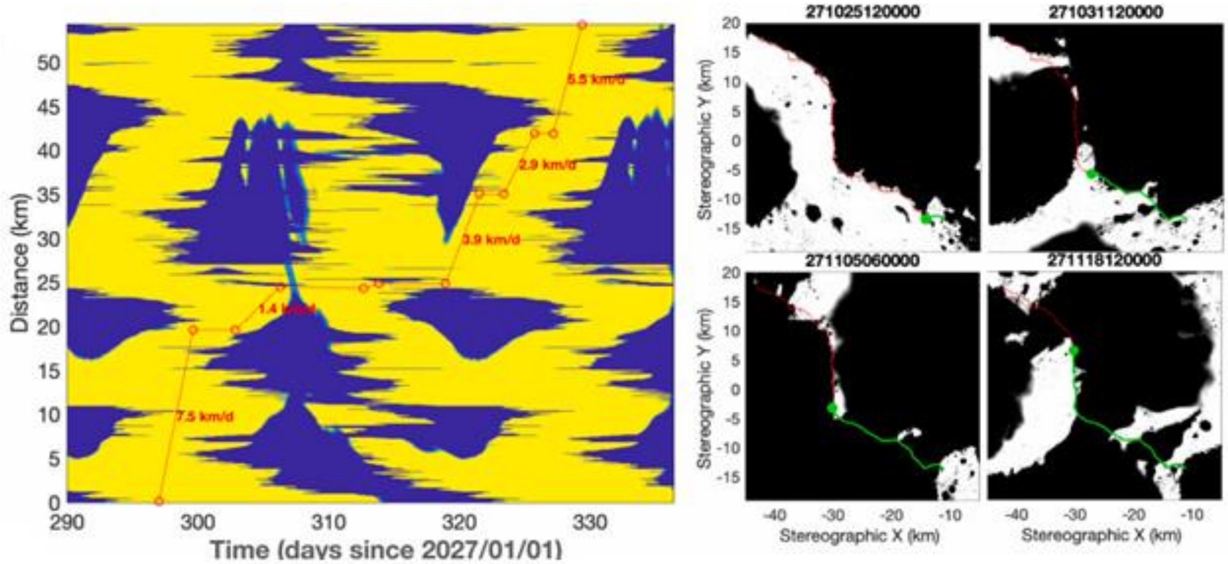

Figure E.2 Illustration of example traverse between the Connecting Ridge and de Gerlache Rim, left shows path illumination matrix (distance vs time), right shows illumination conditions at four times during the traverse (date/time as YYMMDDHHMMSS)

While shorter traverses (less than 10 km) in conjunction with 85-hour shadow survival are possible every month, longer traverses (greater than 10km) with 85-hour shadow survival may only be possible in the lunar summer season to avoid longer shadow periods.

During the winter season, results show illuminated safe havens where the lunar asset could hibernate. A lunar asset could travel away from an illuminated safe haven early in the lunar summer season and return to the safe haven before the winter season.

Increasing survival thresholds from 85 hours to 150 hours expand the illuminated safe havens in the winter season for Connecting Ridge, de Gerlache, Slater. A 150-hour survival threshold decreases hibernation needs during winter season, increases longer traverse potential, and reduces the need for external power to survive. The lunar asset’s independent survival threshold will define the exploration range throughout the year.

Although the provided example was specific to Connecting Ridge and de Gerlache, site selection for lunar assets has not been determined. The expectation is assessments address illuminated safe havens or points of light to successfully reach Artemis science points of interest and commercial objectives.